HHS Public Access

Author manuscript

Invest Radiol. Author manuscript; available in PMC 2017 June 01.

Published in final edited form as:

Invest Radiol. 2016 June ; 51(6): 349–364. doi:10.1097/RLI.0000000000000274.

Sparse Reconstruction Techniques in MRI: Methods, Applications, and Challenges to Clinical Adoption

Alice Chieh-Yu Yang, B.S.[1], **Madison Kretzler, M.S.**[2], **Sonja Sudarski, M.D.**[3], **Vikas Gulani, M.D., Ph.D.**[1,4], and **Nicole Seiberlich, Ph.D.**[1,4]

[1]Department of Biomedical Engineering, Case Western Reserve University, Cleveland, USA

[2]Department of Electrical Engineering and Computer Science, Case Western Reserve University, Cleveland, USA

[3]Institute for Clinical Radiology and Nuclear Medicine, University Medical Center Mannheim, Medical Faculty Mannheim - Heidelberg University, Heidelberg, Germany

[4]Department of Radiology, University Hospitals of Cleveland, Cleveland, USA

Abstract

The family of sparse reconstruction techniques, including the recently introduced compressed sensing framework, has been extensively explored to reduce scan times in Magnetic Resonance Imaging (MRI). While there are many different methods that fall under the general umbrella of sparse reconstructions, they all rely on the idea that a priori information about the sparsity of MR images can be employed to reconstruct full images from undersampled data. This review describes the basic ideas behind sparse reconstruction techniques, how they could be applied to improve MR imaging, and the open challenges to their general adoption in a clinical setting. The fundamental principles underlying different classes of sparse reconstructions techniques are examined, and the requirements that each make on the undersampled data outlined. Applications that could potentially benefit from the accelerations that sparse reconstructions could provide are described, and clinical studies using sparse reconstructions reviewed. Lastly, technical and clinical challenges to widespread implementation of sparse reconstruction techniques, including optimization, reconstruction times, artifact appearance, and comparison with current gold-standards, are discussed.

Keywords

MRI; compressed sensing; sparse reconstruction; non-Cartesian; review; clinical; HYPR; k-t BLAST; L1 SPIRiT; Magnetic Resonance Fingerprinting

Introduction

Magnetic Resonance Imaging (MRI) scans are often long, and it can be challenging and sometimes impossible for patients to comply with long requisite periods of stillness or

Corresponding Author Address: Nicole Seiberlich, Wickenden Building, Rm. 428, 10900 Euclid Avenue, Cleveland, OH 44106, Tel: +1 216 368 6248, Fax: +1 216 844 8062, nes30@case.edu.

breath-hold commands for imaging certain organs. Moreover, rapid motion or contrast changes are difficult to capture with MRI, and any anatomic, physiologic, or contrast media concentration changes that occur during data collection can lead to errors in the resulting images. There are many clinical applications where information from MRI could be useful, but this information cannot be captured accurately with standard MR imaging techniques.

Significant research effort has been directed towards finding ways to accelerate MR imaging. Techniques including the family of parallel imaging reconstruction methods[1–4] have been successful in reducing clinical MRI scan times by factors of two or four, or even higher in some applications[5–8]. These acceleration techniques have also been used to improve image quality or reduce artifacts while maintaining scan time[9,10]. However, the scan time reduction with parallel imaging is limited, and other ways of reconstructing images from undersampled data have been explored, including sparse reconstruction methods such as compressed sensing[11–28].

While compressed sensing has recently received a lot of attention for its potential to accelerate MRI data collection, compressed sensing is just one type of reconstruction which exploits image sparsity to reduce scan time and/or improve image quality. Other sparse reconstruction techniques include partially separable techniques[29–45], k-t methods[46–54] and model based reconstructions[55–74]. At the heart of these sparse reconstructions is the idea that MR images are compressible, or contain redundant information. If the data can be undersampled in such a way that the essential components are still captured, data collection time can be dramatically reduced while maintaining image quality. Because these techniques rely on image sparsity, and not hardware as in parallel imaging, the potential for scan time reduction exceeds that of parallel imaging. Indeed, some groups have shown that sparse reconstruction techniques could be used to generate images that have been accelerated by factors of 225[30] or more[75]. Such high acceleration rates and resulting increased spatial and/or temporal resolution could make possible applications that have traditionally been impossible with MRI. However, while the promise of extremely rapid imaging has driven significant research into sparse reconstruction techniques, many of these methods have fallen short of entering routine clinical practice. When employed for imaging, conservative acceleration rates are often used due to the observation that sparse imaging techniques such as compressed sensing may generate unpredictable artifacts that are highly dependent on the object, potentially interfering with image interpretation. Reconstructions of dynamic datasets which take information from multiple timeframes into account, and which thus have a long “temporal footprint,” may lead to images with inaccurate temporal behavior, also compromising clinical utility. Lengthy reconstruction times and many tunable parameters complicate optimization and assessment for clinical efficacy. Such technical and clinical challenges make clinical adoption of these methods difficult and can only be solved through combined input from MR physicists/engineers and physicians.

This review describes the basic concepts behind sparse reconstruction techniques, how these technologies could be applied to improve MR imaging, and the challenges to widespread implementation of sparse reconstruction techniques from both a technical and clinical perspective.

MRI Data Collection and Acceleration

MRI data are collected in a space that is mathematically related to the image, called k-space. Once the k-space data have been collected, they can then be transformed into an image using the mathematical function that relates the two spaces, the Fourier Transform (as shown in Figure 1a). Collecting a complete set of k-space points can be time-consuming, and there are many situations in which it is desirable to accelerate the data collection process by simply collecting less data, or undersampling the k-space data. However, while undersampling k-space can reduce scan time, it often leads to artifacts in the image.

Artifacts caused by undersampling can take on many forms depending on the sampling scheme. If the data are undersampled such that only every other line of the full k-space were collected, the total scan time is cut in half. However, skipping lines results in aliasing, or fold-over, artifacts in the image (Figure 1b). Other sampling patterns, such as the random undersampling shown in 1c or the radial undersampling in 1d, will result in different types of artifacts. In most cases, the image must be "reconstructed" to eliminate these aliasing artifacts before it can be used clinically. There are several techniques that can be used to reconstruct full images from incomplete data, including the sparse reconstruction techniques that are the topic of this review.

Sparse Reconstruction Techniques

Sparse reconstruction (including methods which fall under the terms constrained reconstructions, compressive sampling, and compressed sensing) is a set of techniques which uses image properties that are known a priori to reconstruct MR images from highly undersampled k-space data. While there are many different types of sparse reconstruction methods, they all share the same overarching goal: To generate an image that is consistent with the data collected which also exhibits specific image properties, determined by the user.

Sparse reconstructions are based upon the combination of three main concepts:

1. Image Sparsity
2. "Noise-like" or benign aliasing artifacts
3. The use of a specialized reconstruction for image recovery

In a "sparse" image, most of the information in the image is contained in small number of image pixels. One example of a sparse MR image is an angiogram, where a few image pixels are bright (with high signal intensity values), and the rest are dark (with low values, ideally zero). Figure 2a shows a sparse MR image, in this case a single partition subtraction image from a 3D abdominal and pelvic contrast-enhanced MR angiogram. If undersampled k-space data are collected, the resulting accelerated image will contain aliasing artifacts and may no longer be sparse; this is the case in Figure 2b. However, if it is known a priori that the fully-sampled image should be sparse, and that the lack of sparsity in the accelerated image is due to aliasing, it may be possible to use a sparse reconstruction to recover the unaliased, sparse image from the undersampled data.

Most MR images are not intrinsically sparse, but as long as the image is sparse in some representation, or domain, a sparse reconstruction can still be used. A sparsifying transform, often denoted by the symbol Ψ, is a reversible user-selected mathematical operation that can be applied to an image to increase sparsity. For instance, the image in Figure 3a, which is not sparse, can be made sparser by applying a spatial finite differences transform, resulting in Figure 3b. The spatial finite differences transform involves calculating the difference between intensity values of neighboring pixels, thereby highlighting edges in the image. Figure 3c shows the sparse image that results from applying a wavelet transform to the image in Figure 3a.

In addition to exhibiting spatial sparsity, some dynamic MR images are temporally sparse, or sparse "through time." An example of such a dynamic dataset is a time series of images showing cardiac motion, as shown in Figure 4a. In this example, only a small subset of image pixels varies through the image series. Such images can be made sparse by subtracting one time frame from the next, as depicted in Figure 4b. The resulting temporal difference image is sparser than the original because only pixels near the heart, where motion occurs, are non-zero. Figure 4c shows how the Fourier transform in the temporal direction can also be used to sparsify dynamic images.

The second requirement for sparse reconstruction techniques is that the true image signal is distinguishable from the aliasing artifacts that arise from undersampling. While sparsity in the image domain is a key feature for sparse reconstructions, it is important to recall that MRI data are collected in k-space. The selection of an appropriate k-space sampling pattern, which determines the appearance of the aliasing artifacts, is also essential to the ability of the sparse reconstruction to generate an acceptable image. Many sparse reconstruction methods rely on using a data sampling pattern that results in incoherent, or "noise-like" aliasing artifacts. With a regular, evenly spaced undersampling pattern where every other line is skipped, the fold-over artifacts are clearly visible and indistinguishable from the true signal (see Figure 1b). However, if k-space is randomly undersampled, the aliasing artifacts look more like noise, and the actual image can be readily distinguished from the artifacts (Figure 1c).

Random undersampling in k-space provides the noise-like aliasing necessary for many sparse reconstruction algorithms. However, the data collection path through k-space must be smooth, and thus for 2D imaging applications, truly random Cartesian undersampling is not realizable. When encoding MRI data for 3D or dynamic 2D datasets, random or pseudo-random sampling can be achieved by appropriately collecting phase encoding lines[4,13,76,77]. In place of random undersampling in 2D, non-Cartesian trajectories including radial[14,78,79], spiral[64,80,81,], and rosette paths[82], among others[83], can be employed. These non-Cartesian paths offer a smooth movement through k-space that can be implemented in practice while also providing noise-like artifacts when undersampled (see Figure 1d for an example of radial undersampling). 3D non-Cartesian trajectories have also been explored, including radial[84] or cone-shaped paths[85]. Some of these sampling trajectories, including 3D radial, lead to such diffuse noise-like artifacts when undersampled at modest levels that it is not necessary to resolve the artifacts, and a specialized reconstruction scheme is not needed[84].

Because the selection of the appropriate trajectory is so important, trajectory optimization for sparse reconstructions is itself an area of research[86,87]

All sparse reconstruction methods make use of sparsity and specialized sampling patterns, but the information used to recover unaliased images varies greatly from method to method. The large number and variety of sparse reconstruction techniques makes it impossible to describe each of them here. However, it is possible to roughly group some of the methods based on their underlying assumptions of the data. It is important to note that there is some overlap between these techniques, and other techniques may not fall into any of these categories. However, the basic ideas of sparse reconstructions can be generally understood by looking at techniques in these four groups:

- Methods which separate spatial characteristics from temporal dynamics (such as RIGR[29] or HYPR[30])
- Methods which separate aliased pixels in the spatiotemporal domain (such as UNFOLD[48] or k-t BLAST[50])
- Compressed sensing techniques (including L1 SPIRiT[13] and k-t SPARSE-SENSE[15])
- Model-based reconstruction methods (including dictionary-based techniques such as Magnetic Resonance Fingerprinting[64] and patch-based methods)

Each of these groups of reconstruction methods will be briefly described below.

Separable Methods

Some of the first sparse reconstruction techniques to be employed used the concept of "partial separability," or the idea that spatial information could be separated from temporal changes in a dynamic series of images. In such methods, aliased or low resolution images which capture rapid temporal dynamics are used together with one or more static high spatial resolution images to generate a dynamic series of images with a high spatial resolution showing the desired contrast changes or motion. Some methods use temporal redundancy only, including MR fluoroscopy[32] as well as view-sharing and keyhole imaging[33–36]. Other more sophisticated methods use both temporal and spatial redundancy to improve the reconstruction. Methods in this group include the early sparse reconstruction technique RIGR[29] as well as HYPR[30] and its variants[37–44]. While these methods do not explicitly enforce sparsity, they do rely on the assumption that few image pixels actually change from frame to frame, and that this change is slow and smooth. In HYPR (shown schematically in Figure 5), it is assumed that the signal intensity changes primarily in the blood vessels during the arrival of the contrast bolus in a contrast-enhanced MR Angiography exam. Following the injection of contrast agent, radial data are collected in such a way that they can be highly undersampled to generate low spatial resolution images with a high temporal resolution (Figure 5, top), or reconstructed together to make one high-resolution static image that does not show contrast dynamics. The high-resolution static image is known as the composite image and it shows the locations of all of the blood vessels (Figure 5, center). While the undersampled dynamic timeframes show many areas of

"bright" signal due to the undersampling artifacts, only the pixels that are also bright in the composite image are actually blood vessels and should be bright in each of the single timeframes. The HYPR reconstruction uses the undersampled dynamic images to weight the composite image to give it the correct contrast for each timeframe. In this way, a high-resolution dynamic time series can be recovered (Figure 5, bottom). More detailed descriptions of these types of techniques can be found elsewhere[31,75].

These partially separable techniques can only be used to accelerate dynamic time series, and they function best when the changes from timeframe to timeframe are small. The application that is most frequently accelerated with such techniques is contrast-enhanced MR Angiography, and acceleration rates of over 800[75] have been reported using separable methods due to the high degree of sparsity in the image series. It may also be possible to accelerate myocardial perfusion[37,38], pulmonary perfusion[40], and ultra-short TE spectroscopy[39] using the ideas of partial separability.

Another group of techniques known as low-rank completion methods uses the idea that the background of the image can be separated mathematically from dynamic portions[58,88–91]. If only a few dynamic components are required to represent signal changes, the signal is sparse in this representation. Although included in the separable methods section, these techniques are typically combined with explicit sparsity constraints in compressed sensing-type reconstructions. Additionally, some such methods can be thought of as model-based techniques if the sparse components make up a dictionary. Such hybrid techniques serve to highlight the complex nature of sparse reconstructions and lack of clear boundaries separating the different groups of methods.

k-t Methods

Like partially separable techniques, k-t methods[46–54] take advantage of the sparsity of a dynamic time series. However, unlike those methods described above, k-t techniques use spatial and temporal sparsity (or joint spatiotemporal sparsity) together instead of separating them. While a detailed review of k-t methods can be found elsewhere[51], this section describes the basic concepts.

In many types of dynamic images, only certain areas of the images contain motion, while other portions remain static. For example, in a cardiac cine image series, it can be assumed that organs other than the heart do not move substantially during the imaging process. This can be seen by looking at an x-t plot of the dynamic images, or the cross-section which shows changes in the images through time (Figure 4c). In the so-called x-f space, which is calculated by applying the Fourier transform through time, only portions of the image that move will lead to signal spread (indicated with the purple arrow); pixels with no motion will be confined to a single pixel (indicated with the orange arrow). This property makes the x-f space sparse in imaging applications were few pixels change over time. If the accelerated k-space data are undersampled in an interleaved fashion, the aliasing in the images appears as distinct and often non-overlapping replicas in the x-f space. k-t methods, which include techniques such as UNFOLD[48] and k-t BLAST/SENSE[50], rely on the separation of these replicas in the x-f space for reconstruction.

UNFOLD uses a low-resolution training dataset to determine what the signal should look like in the full x-f space, and then filters the accelerated x-f space to remove the aliasing artifacts. k-t BLAST[50] instead takes the approach of resolving the copies by determining an unmixing matrix using the low-resolution time series, which can provide a more nuanced reconstruction of signals in the x-f space. Figure 6 illustrates the basic idea of k-t BLAST. Aliasing from interleaved undersampling can be seen in the accelerated data in x-f space (Figure 6c, top), but with knowledge of the structure of the true x-f profile (dotted line in Figure 6c, bottom), a set of unaliased images can be generated (Figure 6e). k-t SENSE is a form of k-t BLAST in which parallel imaging is incorporated to help resolve aliased pixels, enabling higher acceleration factors to be employed. Other k-t variants exist, including those that involve parallel imaging in a different way or use sparsifying transforms other than the temporal Fourier transform[52–54].

The various k-t methods provide the ability to accelerate dynamic acquisitions. However, they only work for dynamic time series and perform best when motion is smooth and limited to a subsection of the image. These methods have been applied to cardiac functional and perfusion imaging[49,50,53,54] and fMRI[48] but have the potential to be used in any case which meets these requirements. Additionally, k-t methods are often combined with other types of sparse reconstruction techniques, such as the compressed sensing-based k-t FOCUSS[47] and k-t SPARSE[28].

Compressed Sensing

Although sparsity has been exploited to accelerate MR imaging for many years, sparse reconstructions regained popularity after the introduction of compressed sensing (also known as compressive sampling)[11,12]. The basic idea of compressed sensing is that if MRI data are collected such that the undersampling artifacts appear as noise (incoherent aliasing) and the images are sparse, the full image can be recovered using an appropriate non-linear reconstruction method. These nonlinear reconstruction techniques enforce two conditions:

1. Sparsity of the image in the transform domain
2. Consistency of the reconstruction with the acquired data

The first condition enables aliasing artifacts to be separated from actual signals in the image by requiring that the reconstructed image is sparse (or sparse in the transform domain). The second condition ensures that the reconstruction does not replace actual acquired data with arbitrary data in the interest of making the final solution sparse. Thus these two requirements balance the desire for a sparse image, and an image that is consistent with the data collected.

This problem can be formulated mathematically using the following minimization:

$$\text{minimize} \|F_u m - y\|_2^2 + \lambda \|\Psi m\|_1 \quad (1)$$

where Ψ is a sparsifying transform chosen by the user to convert the image m into a sparse domain, y are the actual undersampled k-space data acquired, and F_u is the Fourier transform for the data collection trajectory that was employed. The first term ensures that the

reconstructed image m is consistent with the k-space data that have been collected, y. This term calculates the least-squares difference, denoted as $\|\bullet\|_2$, between the k-space of the reconstructed image and the k-space that was acquired. The second term ensures that the reconstructed image m is sparse in the selected transform domain. This term uses the L1 norm, $\|\bullet\|_1$, which calculates the degree of sparsity in the image by summing the absolute value of the pixels in the image (or the image after the sparsifying transform). Thus, described in words, this equation seeks to find an image m which is both sparse (or transform sparse) and also consistent with the data that has been collected The so-called regularization parameter, λ, controls the relative importance of the two terms in the reconstruction. Selecting a small value of λ will lead to a solution that is closer to the collected data and relies less on the sparsity term, whereas a large value of λ will lead to a final image that may deviate from the collected data in the interest of providing a sparse solution.

A schematic example of a basic compressed sensing algorithm is shown in Figure 7. The gray box shows how the algorithm iterates between enforcing sparsity (top row) and ensuring data consistency (bottom row). Note that there are much more elegant and efficient techniques which can be used to solve these minimization problems, for instance projections onto convex sets or iterative soft thresholding.

Unlike the methods described in the previous sections, compressed sensing can be used to accelerate static images by using only spatial transforms, or temporal transforms can be included when reconstructing accelerated dynamic data. Parallel imaging is often incorporated into these techniques to further increase the data reduction factor and improve image quality[13,15,18]. Because motion, including cardiac and respiratory motion, can reduce the efficacy of compressed sensing reconstructions, a number of groups have incorporated navigator information[19–21], image registration[22–24], or even an additional motion dimension[25,26], directly into the reconstruction.

An example of a static compressed sensing reconstruction is L1 SPIRiT[13] which uses the parallel imaging method SPIRiT[4] combined with a spatial wavelet transform to sparsify the images. L1 SPIRiT is an iterative reconstruction that is typically used with 3D Cartesian datasets collected using a pseudo-random Poisson disk sampling pattern. This technique has the potential to accelerate clinical MRI scans by a factor of 8 in applications such as pediatric body imaging[13,27].

k-t SPARSE-SENSE[15] is a compressed sensing method which takes advantage of sparsity in the spatiotemporal domain by using a temporal total variation transform. This technique has been used for high frame rate dynamic cardiac imaging, angiography, and free-breathing liver imaging with acceleration factors up to 8. GRASP[14] (Golden-Angle Radial Sparse Parallel) is a version of k-t SPARSE-SENSE which works with radial data collected in a continuous fashion for dynamic 3D imaging. GRASP has been demonstrated in dynamic contrast-enhanced free-breathing liver, pediatric body, breast, and neck imaging with acceleration factors up to 28.7.

While L1 SPIRiT and k-t SPARSE-SENSE/GRASP have been used as examples of compressed sensing techniques in this section, there are many more compressed sensing type reconstruction algorithms that have been presented in the literature and reviewed elsewhere[92,93].

Model-Based Methods

Model-based methods are another type of sparse reconstruction technique which make the assumption that the final image or time series can be described using a set of parameters that is much smaller than the total number of image pixels, which would indicate that the data are redundant and can tolerate high degrees of undersampling. For instance, in the case of T_1 relaxation parameter mapping, a time course made up of several T_1 weighted images is usually collected and used to determine the T_1 value for each pixel by performing a mathematical fit (Figure 8a and 8b). However, although many T_1 weighted images are collected to yield an accurate value of T_1, only two unknowns actually must be determined for each pixel, the proton density and T_1. Thus, a dictionary of possible time courses for the T_1 weighted images can be determined mathematically; these are the only possible time courses that can be found in the images (excluding noise), as the physics of T_1 relaxation are well understood (Figure 8c). If the images in the time course are randomly undersampled, this dictionary can be used to recover the T_1 maps despite the aliasing that results from the accelerated scan (Figure 8d and 8e).

There are different ways of using a model to perform a sparse reconstruction. For instance, some sparse reconstruction techniques employ the dictionary of possible elements as a sparsifying transform in a compressed sensing reconstruction[55,59–63]. MR Fingerprinting[64] is a dictionary-based approach in which highly undersampled pixel time courses are matched to a dictionary of possible time courses to derive T_1 and T_2 maps. While MR Fingerprinting does not rely on the image time series itself to be sparse, this method uses the idea that a sparse set of dictionary elements, in this case a single element, can be used to represent the time course of each pixel. Yet other techniques employ a signal model directly in the reconstruction to constrain the resulting images or time courses to follow a specific mathematical form[94–98]. Such a parametric approach does not require the user to explicitly calculate all of the possible elements to form a dictionary, which may allow improved results as any values of the model parameters can result from the reconstruction (and not just those found in the dictionary). Although the example of T_1 mapping has been used here, any other physical property can be treated in the same manner if a well-defined mathematical relationship exists between the signal time course and the property to be measured, such as T_2 [65], proton density[56], fat fraction[95–98], or susceptibility mapping[94]. Additionally, there are methods which use the images themselves to determine an appropriate signal model; here an explicit knowledge of the mathematical model is not required[59,61,66].

In addition to using mathematical models to depict signal time courses, some sparse reconstruction techniques use spatial “patches” to model the information in MR images[67–74]. Such methods assume that each block of pixels in an image can only be described by the elements in a dictionary of possible blocks. These possible blocks are determined either empirically or using a priori information such as a set of similar images.

These techniques can use 2D[70,71] or 3D blocks [72,73], and can even be combined with time course modeling methods for further sparsification[58,69].

Clinical Applications of Sparse Reconstruction Techniques

A sparse reconstruction technique is often directed towards accelerating a particular application, such as dynamic cardiac or abdominal imaging, MR angiography, or high-resolution brain imaging. The performance of the technique is then demonstrated in a small set of proof-of-concept reconstructions using in vivo data, typically collected from healthy volunteers and sometimes a small number of patients. However, the impact of the various sparse reconstruction techniques in clinical practice with regard to diagnostic accuracy has been less extensively studied[93]. The following section describes some applications where sparse reconstructions hold clinical promise. The literature reviewed is representative, but by no means exhaustive.

Vascular and Flow Imaging

MR angiograms are relatively sparse in the image domain and can be further sparsified in both the image domain and in the time domain. Therefore, MR angiography (MRA) is a natural application for sparse reconstructions. Both contrast enhanced[99] and non-contrast enhanced MRA[100] have been examined in a variety of applications, including intracranial vasculature[101,102], carotids[103,104], coronaries[19], and pulmonary veins[105]. Reducing the acquisition time enables the dynamic visualization of the flow of blood sequentially into arteries and then veins via repeated rapid imaging. This may allow the characterization of pathologies such as abnormal blood flow dynamics and arteriovenous malformations[106].

The challenge of collecting angiograms in regions where the degree of physiological motion encountered requires high temporal resolution imaging to capture the anatomy or the contrast bolus during peak enhancement has also driven the development of fast imaging methods. Pulmonary angiography, thoracic angiography, and coronary angiography are important representative techniques in which respiratory and cardiac motion pose major difficulties, necessitating ultrafast imaging[19,85,105,107–109]. Abdominal MR angiography poses the twin challenges of rapid contrast dynamics and a need for very large field of view coverage. Thus significant efforts to use sparse reconstruction techniques for acceleration in the abdomen are underway, both in adults and children[110].

The use of sparse reconstructions has also been explored for improving 4D flow or phase contrast imaging[111], to evaluate valvular insufficiency, improve accuracy in delineating shunt pathology, assess anomalous flow in pulmonary veins, and visualize hemodynamics in congenital heart disease[112–116]. Sparse reconstructions have been used to obtain single breath-hold characterization of portal flow[117] and can yield improved vessel conspicuity while retaining accuracy of quantification of portal flow[118]. While the carotid vasculature does not pose the same motion problems as thoracic and abdominal regions, the very high resolutions needed for vessel wall imaging in these regions necessitate extremely long acquisitions (8–10 minutes are not unusual). Early exploration of sparse reconstructions in this setting in volunteers and two patients shows greater than 8-fold acceleration of the exam with improved flow quantification[119].

Cardiac Imaging

Cardiac examinations are some of the longest MRI protocols and are dependent on patient compliance and the patient's ability to hold his or her breath. Technologies for accelerating cardiac imaging using sparse reconstructions are being explored for free-breathing cine imaging[23,120–124] and for breath-held functional assessment of measurements such as left ventricular volume, ejection fraction, and mass[125–127]. The largest study included 21 patients and showed that single accurate breath-hold functional measurements are feasible in patients with a variety of cardiac pathologies[126]. Multiple groups are exploring the application of sparse reconstruction techniques to first pass perfusion imaging[15,128–132] in pathologies such as atrial fibrillation, where it was previously impossible to obtain diagnostic exams[133]. Such advances could contribute to a highly efficient and rapid throughput approach that could greatly simplify cardiac MR[134]. However, questions remain regarding image quality compared to traditional exams[134] and whether CS-based methods suffer from worsened spatiotemporal blurring compared to parallel imaging-based acceleration[135,136]. Acceleration of late gadolinium enhancement (LGE) exams with sparse reconstructions for faster/free breathing acquisitions or greater anatomical coverage has also been explored[136–138]. An early study of 3D isotropic LGE imaging on 28 patients indicates that accelerated scans may be used to visualize left ventricular scar with a high spatial resolution, and potentially pulmonary vein and left atrial scar post ablation for atrial fibrillation[137].

Abdominal and Pelvic Imaging

Abdominal imaging requires large fields-of-view for organs such as the liver, or entire abdominal/pelvic cavity for imaging the bowel for applications such as enterography, while retaining sufficient resolution for visualization and characterization of pathology. Children have particular difficulty in providing the long breath-holds required; these patients are scared and often sedated or anesthetized. Thus application to pediatric abdominal imaging is one of the first areas where early application of sparse reconstructions such as compressed sensing has been particularly promising, for improved delineation of key structures in the abdomen with significantly shortened acquisition times[14,20,79,139,140].

Abdominal perfusion imaging in kidneys and liver is particularly challenging for quantitative analysis due to the need for dynamic imaging of large fields-of-view at a high resolution. Ultrafast imaging techniques, including the family of sparse reconstruction techniques discussed here, are potentially enabling technologies for robust abdominal perfusion analysis with improved 3D coverage. Application of compressed sensing acquisitions has been reported for quantitative renal and hepatic perfusion imaging[141,142] with volumetric coverage and high spatial resolution. Similarly for MR enterography in Crohn Disease, a free-breathing accelerated acquisition could be used to enable perfusion measurements in addition to qualitative imaging of terminal ileitis, opening the door for quantitative analysis[143]. Accelerated DCE imaging of the prostate with quantitative perfusion characterization has also been explored[144].

Fat and water imaging plays an important role in the abdomen and multiple groups have accelerated these acquisitions using sparse reconstructions[96–98,145]. Faster imaging to reduce

breath-hold lengths could lead to improved image quality, and acceleration for this purpose has been demonstrated[146,147] and used for measurement of hepatic steatosis in diabetic patients without compromising accuracy of measurement[147]. Quantitative measurement of relaxation times in the upper abdominal organs with Magnetic Resonance Fingerprinting has also been explored, and early work indicates that colorectal cancer hepatic metastases can be differentiated from surrounding parenchyma[148].

MR Spectroscopic Imaging (MRSI) has potential in characterizing tumors in the prostate, but long acquisitions are required, which can be clinically prohibitive. Recent advances have shown that sparse reconstructions can be used to significantly reduce these acquisition times while providing quantitative information on multiple relevant metabolites. It remains to be seen whether such advances can make the technique more feasible for routine clinical application[149].

Neuroimaging

As in other anatomical regions, sparse reconstructions could be used in neuroimaging to enable exams that have traditionally been too long for practical use. For example, arterial spin labeling (ASL), a non-contrast method for measuring perfusion, can be made significantly faster and yet more accurate using sparse reconstructions[150]. Similarly, accelerated dynamic contrast-enhanced imaging has been achieved for accurate characterization of brain perfusion parameters[151]. Accelerated scans have been used for qualitative and quantitative analysis of pituitary adenomas[152]. As with prostate, spectroscopic imaging can be shortened and made more feasible[153] for assessment of pathologies such as obstructive sleep apnea[154], which have been shown to be associated with biochemical alterations of multiple metabolites. Applications of quantitative relaxometry technologies such as MR Fingerprinting indicate that subtle but measurable region-specific aging-related changes may occur[155], leading to the possibility of using relaxation time changes to assess diffuse pathologies and potentially focal lesions.

Functional MRI (fMRI) is a challenging application requiring rapid imaging and quantitative characterization of very small signal changes. Sparse reconstruction approaches have been used to accelerate fMRI exams while still providing high quality activation maps in areas of low SNR[156] and improved sensitivity to functional activation[81]. Sparse imaging has also been employed to reduce susceptibility artifacts in fMRI and improve imaging efficiency, making use of the fact that hemodynamic signal changes in fMRI are typically small from frame to frame[157].

A major area of development within neuroimaging is diffusion tensor imaging (DTI). For applications such as high angular resolution diffusion imaging (HARDI), a very large number of high spatial resolution images must be obtained, which result in long acquisition times. Acceleration with sparse reconstruction techniques is being actively explored improve these q-space or HARDI acquisitions[158–161]. In addition to tractography and basic neuroanatomical research, these technologies have application in accelerating fiber tracking around tumors for surgical planning[162].

Lung Imaging

The high temporal resolution acquisitions enabled through modern reconstruction techniques are starting to make pulmonary MRI a feasible alternative to CT, and a number of groups are exploring the utility of sparse reconstruction techniques for imaging lung structure and function. Enabling the use of MRI for rapid and high-resolution structural assessment of the lungs, for instance in children with cystic fibrosis, could reduce the large burden of radiation associated with repeated CT scans. In a review exploring MR imaging for lung cancer screening, it has been suggested that compressed sensing may provide some of the acceleration needed for MR to image small tumors in the lungs[163]. Another developing area of clinical interest has been imaging of the lungs and lung function using hyperpolarized ^{3}He imaging[164]. Acceleration enables accurate calculation of ventilation, with initial application in imaging ventilation changes in asthma[165]. The same group has previously explored hyperpolarized ^{3}He for chronic obstructive pulmonary disease (COPD)[166] and application to this pathology is also likely feasible. Alternatively, an ultrashort echo time (UTE) approach has been used with compressed sensing for imaging COPD patients, where UTE MR signal intensity correlates to CT density and can be related to pulmonary function metrics such as FEV1/FRC[167].

Musculoskeletal Imaging

While imaging of joints such as the knee is not intrinsically complicated by motion, many patients, especially children, have difficulty laying still for the entire exam. Early clinical implementations of sparse reconstructions for clinical use thus included imaging the knee for the pediatric population[140]. Sparse reconstructions may make it possible to image areas such as the cartilage in the hip, which can be as thin as 1–2 mm, at higher spatial resolution in a given scan time. An area of particular interest in musculoskeletal radiology is the development of technologies that enable imaging near metal. Multispectral imaging approaches for imaging around metal can be accelerated using sparse reconstruction techniques, without loss of image quality, in clinically relevant settings such as patients with implanted spinal fixation hardware[168]. Spectroscopic imaging of areas such as the calf[169] may also be feasible with the increases in imaging speed afforded by sparse reconstruction techniques.

High field sodium imaging of cartilage holds promise because it could help quantify glycosaminoglycan content, which in turn could relate to the degree of cartilage degradation in early osteoarthritis. It has been shown that sparse reconstructions can be used for faster and yet accurate quantitative sodium imaging of knee cartilage at 7T, opening the door for sodium imaging-based quantitative assessment of osteoarthritis[170]. Quantification of $T_{1\rho}$ similarly holds promise for characterization of osteoarthritis, and acceleration of $T_{1\rho}$ mapping in the knee has been demonstrated in early feasibility studies[171,172]. Accelerated dynamic functional metabolic imaging of phosphocreatine kinetics after calf muscle exercise has also been shown for 3D ^{31}P spectroscopic imaging at 7T[173]. Such technology could be used to study exercise physiology and also pathology related to altered bioenergetics in skeletal muscle. Accelerated fat fraction with incorporation of effects of R2* has been demonstrated for improving accuracy in fat fraction mapping in musculature of patients with

Becker muscular dystrophy, with implications for clinical trials where such quantification is needed[174,175].

Technical Challenges

While sparse reconstruction techniques show promise in many MR applications, the selection and optimization of an acceleration technique for a given application is both technically and clinically challenging. Before a method can replace the current clinical standard-of-care technique, significant testing must be performed. In the best cases, this testing is difficult and time-consuming, and in the worst case, nearly impossible to perform due to the need for repeat patient scans. Moreover, the results of comparisons between sparse reconstruction techniques and more commonly-employed acceleration methods can yield different results depending on the specific application, reconstruction techniques that are examined, and method of comparison. Some groups have reported advantages when replacing conventional imaging methods with sparse reconstruction techniques[25,109,114,162,176,177], while others have seen that standard clinical techniques continue to outperform these novel methods[135,178]. These conflicting reports stem from the challenges that basic scientists and clinicians alike face when employing sparse reconstruction methods. The following sections examine some of these challenges associated with both testing sparse reconstructions in a research setting as well as using sparse reconstructions in a clinical setting.

A major obstacle faced by researchers is that it is difficult to compare the quality of various reconstruction approaches, as the true test of a reconstruction is the diagnostic value of the resulting images. However, it is clearly not feasible for radiologist to assess the results of every reconstruction technique under development, and thus proxy metrics are often used. In some studies, authors calculate an “image error” metric by comparing the results of their image reconstruction to gold-standard images where all the data can be collected[86,175,179]. However, the ability of the reconstruction technique to enable visualization of specific pathology and anatomy are far more important to a radiologist than a mathematical match to what might also be a flawed gold-standard. Thus, while the use of these metrics simplifies the comparison of techniques in a research setting, these analyses may lead to methods that do not translate well to clinical practice. Overall image quality or feature conspicuity as rated by a radiologist may be preferable[140,168,180] but even these are proxies for a true comparison of diagnostic accuracy in a clinical setting.

A second challenge is that the performance of each method depends strongly on the parameters used in the reconstruction. For instance, in compressed sensing reconstructions, a number of different sparsifying transforms beyond finite differences and wavelets have been proposed, including but not limited to singular value decomposition [181], principal component analysis[53,151], Haar[182] and temporal Fourier transforms[182]. To complicate matters, some proposed compressed sensing implementations use more than one sparsifying transform[151,182]. Once the number and type of sparsifying transforms have been selected, it is often necessary to determine an appropriate value for the regularization parameter associated with each transform. The results of the sparse reconstruction depend highly on the choice of the regularization parameter(s). Figure 9 demonstrates how an improperly

tuned regularization value can lead to an image that has lost many essential features, as the sparsifying transform has been overemphasized. The optimal value of the tunable parameter(s) can be drastically different between methods, and while it may be possible to determine suitable parameters for an application through extensive testing[183], these parameters will apply only for that application[184]. Some groups have attempted to move to techniques which do not require an adjustable regularization parameter[185,186], but the relative performance of these methods has not been assessed.

In addition to the regularization parameter, the performance of many sparse reconstruction methods is highly dependent on the way that the MRI data are sampled and the degree of undersampling. Often retrospective undersampling is employed for testing, as only one dataset must be collected and simply downsampled with different sampling patterns. However, the behavior of the magnetization may be different when collecting accelerated data than it was when collecting fully-sampled data due to the underlying physics[87]. Thus, the sampling pattern and acceleration rate that are found to be optimal with retrospectively undersampled data may not be the same for prospectively undersampled data. However, to collect prospectively undersampled data with different sampling patterns and acceleration factors, many more actual experiments must be performed, which is both expensive and time-consuming.

Another challenge is that most sparse reconstruction methods use complicated algorithms which can be difficult to implement. While researchers are able to develop and expand upon their own techniques, they may not be able to properly implement the techniques of others, even after the methods have been published. This makes unbiased comparisons of different sparse reconstruction techniques nearly impossible. However, there have been several attempts to help make fair and appropriate comparisons, which typically fall under the term “reproducible research”. For instance, there has been a push in the scientific community to deposit reconstruction code in code repositories, such as “MRI Unbound” [187] or the fat-water toolbox that is available online as part of the ISMRM Workshop “Fat-Water Separation: Insights, Applications & Progress in MRI”[188]. Code in these repositories can then be downloaded by others for comparison purposes. Another option for algorithm comparison is a so-called “reconstruction contest,” in which a research society provides a dataset that is available for download. Multiple research groups can use their own techniques to reconstruct the images, which are then uploaded back to the society and then compared either quantitatively to a gold-standard image, qualitatively by radiologists, or both, to determine the “best” reconstruction method. For instance, in such a contest sponsored by ISBI 2012, 20 different reconstruction algorithms were tested using HARDI data and the results compared in terms of image quality and quantitative accuracy[189]. In this contest, none of the methods was found to significantly outperform the others in all experimental conditions, further highlighting the challenge in selecting just one for clinical adoption.

Because many sparse reconstruction techniques are computationally intensive, the generation of images using these techniques can take a significant amount of time. Reconstruction times on the order of hours or even days have been reported[14,42,72,151]. Such long reconstruction times make it difficult to test the relative performance of different methods or determine optimal parameters. Many groups have moved to using dedicated

image reconstruction platforms which employ hardware and code optimized for rapid computations[190]. The use of specialized hardware and implementations including Graphics Processing Units (GPUs)[27,191], distributed computing[192], and/or multicore processors[193] has been shown to enable 50-fold reductions in computation time, making clinical application of these sparse reconstruction techniques feasible[191].

Challenges to Clinical Application

In addition to the technical challenges associated with sparse reconstruction techniques, there remain significant clinical barriers to widespread testing, let alone adoption, of these methods. Ultimately, the success of a technique such as sparse image reconstruction depends on its acceptance by the radiology community, as these physicians are the end users of the technology. Full validation of new imaging methods must demonstrate diagnostic accuracy, or equivalent accuracy at a reduced scan time. Unfortunately, such validation is a lengthy and challenging process as it must show that the new imaging technology not only produces images of higher quality based on quantitative metrics, but also impacts clinical care in a meaningful way.

A major barrier to clinical adoption is that the imaging community has relatively little experience with the artifacts that can arise from these sparse reconstruction techniques. For example, the artifact profile with compressed sensing has been described to include significant image blurring and a “global ringing” similar in appearance to motion ghosting, and these can have deleterious effects even at a two-fold acceleration[180]. Furthermore, since many of these technologies take advantage of image information collected over a wider time window than a single frame of the imaging time series, it is possible that “temporal” artifacts are produced; in other words, each individual image may be acceptable, but the temporal fidelity with which events are observed in the imaged anatomy may be compromised. While the presence of artifacts in any accelerated image is an expected phenomenon, the unfamiliar and unpredictable nature of these artifacts means that radiologists or technologists may not be able to troubleshoot or even recognize them. This problem can be compared to the use of iterative reconstruction methods for reducing the radiation dose in Computed Tomography. The images generated with these new approaches look different than those reconstructed with more traditional filtered back projection approaches, and in many cases while they have less noise, the iterative reconstruction techniques may in fact obscure pathology[194]. Due to the large number of parameters in an MRI pulse sequence and contrasts which can be created, this challenge is compounded in MRI.

Another important problem with sparse reconstruction techniques is that of long image reconstruction times; while this creates technical challenges as described above, it can also hinder the use of such technologies clinically. Even if data are collected in real-time, the reconstructed images may not be clinically helpful if they are only available for review hours later. If the reconstruction is not successful due to an incorrect sampling pattern or overly ambitious acceleration rate, the patient would need to return for a second scan. Some patients may be too sick or lack proper transportation to return for repeat imaging, and the cost of repeat scanning may be prohibitive. If there are acutely important findings in the images, the reconstruction time could effectively delay or even preclude treatment. Such

practical considerations may make it difficult to replace current clinical standard exams with the computationally intensive techniques, no matter how enticing their potential benefits are.

Another complication is that testing sparse reconstruction techniques against a clinical gold standard can be problematic. Ideally head-to-head comparisons in non-contrived clinical settings are needed. Some exams, especially dynamic contrast-enhanced series, may be difficult or even impossible to repeat. Even if repeated, it may be challenging to replicate the scan on two different dates or time points. Thus testing of diagnostic utility against an accepted standard may not always be possible. Indeed, such testing in a clinical environment has been performed only with small groups of patients at advanced research hospitals due to the demanding nature of these studies[113,139,180]. True blinded comparisons are further complicated by the fact that the scans to be tested appear clearly different than the clinical standard in terms of SNR, imaging features (i.e. edges, contrast), and artifact profile.

Finally, in some applications, even promising sparse reconstructions may not deliver higher acceleration rates or improved image quality over existing (and emerging) techniques. Multislice[195,196], 3D CAIPIRINHA[197,198], and non-Cartesian parallel imaging techniques[199] enable rapid imaging in many of the clinical applications discussed above, often at acceleration factors which are similar to those used in sparse reconstruction methods. Only a demonstrated dramatic increase in diagnostic efficacy can motivate the decision to use a time-consuming and complex sparse reconstruction technique instead of either the current gold-standard methods or another simpler emerging technology.

Conclusion

Sparse reconstructions, including but not limited to the family of compressed sensing techniques, have the potential to significantly accelerate MRI scans. In this review, the fundamental ideas behind sparse reconstruction methods have been introduced. While many different types of sparse reconstruction techniques have been proposed, all rely on image sparsity, noise-like or benign aliasing artifacts, and the use of a specialized reconstruction. This review also describes the principles of four basic categories of sparse reconstruction techniques, namely separable methods, k-t methods, compressed sensing, and model-based methods. Each of these techniques places different requirements on the collected data and exploits different aspects of the underlying images, and thus some techniques may be better suited to the acceleration of a specific imaging application than others.

While decreasing imaging time for standard exams may be possible using sparse reconstructions, the true benefit of these techniques will be realized if new applications can be enabled through faster imaging. Additionally, it may be possible to better scan patient populations that have traditionally been challenging to image with MRI, including children or patients who cannot hold their breath, thus expanding the role of MR in diagnostic imaging. Despite this great potential, sparse reconstruction techniques have not been widely adopted in the clinic. In order to make such adoption possible, it is essential for researchers and clinicians to work closely together to design, optimize, validate and compare these sparse reconstruction techniques and competing methods. The few studies which have explored the use of sparse reconstructions in a clinical setting typically recommend factors

of 2 to 4 for static imaging, and up to 8 to 12 for dynamic imaging. At these data reduction factors, it will be important to demonstrate the benefit of moving to the more complex and time-consuming sparse reconstruction technique instead of relying solely on parallel imaging, which is well-accepted clinically and broadly used. Thus far, the majority of the work on sparse reconstruction algorithms has been performed by integrated teams of researchers and physicians in academic settings. More general acceptance and routine utilization will require the reconstructions to be rapid and predictable, such that technologists or radiologists can understand and troubleshoot any residual artifacts and either re-reconstruct the data or recollect images while the patient is still on the table.

Acknowledgments

Sources of support: This material is based upon work supported by the National Science Foundation Graduate Research Fellowship Program under Grant No. DGE-1451075, NIH Interdisciplinary Biomedical Imaging Training Program, NIH T32EB007509 administered by the Department of Biomedical Engineering, Case Western Reserve University, NHLBI R01HL094557, NIDDK R01DK098503, NIBIB R01EB016728, NIBIB R01BB017219, and Siemens Medical Solutions.

References

1. Deshmane A, Gulani V, Griswold MA, et al. Parallel MR imaging. J Magn Reson Imaging. 2012; 36(1):55–72. [PubMed: 22696125]
2. Pruessmann KP, Weiger M, Scheidegger MB, et al. SENSE: sensitivity encoding for fast MRI. Magn Reson Med. 1999; 42(5):952–962. [PubMed: 10542355]
3. Griswold MA, Jakob PM, Heidemann RM, et al. Generalized autocalibrating partially parallel acquisitions (GRAPPA). Magn Reson Med. 2002; 47(6):1202–1210. [PubMed: 12111967]
4. Lustig M, Pauly JM. SPIRiT: Iterative self-consistent parallel imaging reconstruction from arbitrary k-space. Magn Reson Med. 2010; 64(2):457–471. [PubMed: 20665790]
5. Aandal G, Nadig V, Yeh V, et al. Evaluation of left ventricular ejection fraction using through-time radial GRAPPA. J Cardiovasc Magn Reson. 2014; 16:79. [PubMed: 25315256]
6. Deng W, Zahneisen B, Stenger VA. Rotated stack-of-spirals partial acquisition for rapid volumetric parallel MRI. Magn Reson Med. Aug.2015
7. Kukuk GM, Hadizadeh DR, Gieseke J, et al. Highly undersampled supraaortic MRA at 3.0 T: initial results with parallel imaging in two directions using a 16-channel neurovascular coil and parallel imaging factors up to 16. Magn Reson Imaging. 2010; 28(9):1311–1318. [PubMed: 20692783]
8. Wright KL, Chen Y, Saybasili H, et al. Quantitative high-resolution renal perfusion imaging using 3-dimensional through-time radial generalized autocalibrating partially parallel acquisition. Invest Radiol. 2014; 49(10):666–674. [PubMed: 24879298]
9. Henzler T, Dietrich O, Krissak R, et al. Half-Fourier-acquisition single-shot turbo spin-echo (HASTE) MRI of the lung at 3 Tesla using parallel imaging with 32-receiver channel technology. J Magn Reson Imaging. 2009; 30(3):541–546. [PubMed: 19711408]
10. Lum DP, Busse RF, Francois CJ, et al. Increased volume of coverage for abdominal contrast-enhanced MR angiography with two-dimensional autocalibrating parallel imaging: initial experience at 3.0 Tesla. J Magn Reson Imaging. 2009; 30(5):1093–1100. [PubMed: 19856443]
11. Lustig M, Donoho D, Pauly JM. Sparse MRI: The application of compressed sensing for rapid MR imaging. Magn Reson Med. 2007; 58(6):1182–1195. DOI: 10.1002/mrm.21391 [PubMed: 17969013]
12. Donoho DL. Compressed sensing. IEEE Trans Inf Theory. 2006; 52(4):1289–1306.
13. Lustig M, Alley M, Vasanawala S, et al. ℓ1-SPIRiT: Autocalibrating parallel imaging compressed sensing. Proc Int Soc Magn Reson Med. 2009:379.

14. Feng L, Grimm R, Block KT, et al. Golden-angle radial sparse parallel MRI: combination of compressed sensing, parallel imaging, and golden-angle radial sampling for fast and flexible dynamic volumetric MRI. Magn Reson Med. 2014; 72(3):707–717. [PubMed: 24142845]
15. Otazo R, Kim D, Axel L, et al. Combination of Compressed Sensing and Parallel Imaging for Highly Accelerated First-Pass Cardiac Perfusion MRI. Magn Reson Med. 2010; 29(3):997–1003. DOI: 10.1002/mrm.22463
16. van Gorp JS, Bakker CJG, Bouwman JG, et al. Geometrically undistorted MRI in the presence of field inhomogeneities using compressed sensing accelerated broadband 3D phase encoded turbo spin-echo imaging. Phys Med Biol. 2015; 60(2):615–631. [PubMed: 25548990]
17. Lingala SG, DiBella E, Jacob M. Deformation corrected compressed sensing (DC-CS): a novel framework for accelerated dynamic MRI. IEEE Trans Med Imaging. 2015; 34(1):72–85. [PubMed: 25095251]
18. Sung K, Hargreaves BA. High-frequency subband compressed sensing MRI using quadruplet sampling. Magn Reson Med. 2013; 70(5):1306–1318. [PubMed: 23280540]
19. Moghari MH, Akçakaya M, O'Connor A, et al. Compressed-sensing motion compensation (CosMo): a joint prospective-retrospective respiratory navigator for coronary MRI. Magn Reson Med. 2011; 66(6):1674–1681. [PubMed: 21671266]
20. Cheng JY, Zhang T, Ruangwattanapaisarn N, et al. Free-breathing pediatric MRI with nonrigid motion correction and acceleration. J Magn Reson Imaging. 2015; 42(2):407–420. [PubMed: 25329325]
21. Chen X, Salerno M, Yang Y, et al. Motion-compensated compressed sensing for dynamic contrast-enhanced MRI using regional spatiotemporal sparsity and region tracking: block low-rank sparsity with motion-guidance (BLOSM). Magn Reson Med. 2014; 72(4):1028–1038. [PubMed: 24243528]
22. Royuela-Del-Val J, Cordero-Grande L, Simmross-Wattenberg F, et al. Nonrigid groupwise registration for motion estimation and compensation in compressed sensing reconstruction of breath-hold cardiac cine MRI. Magn Reson Med. May.2015
23. Usman M, Atkinson D, Odille F, et al. Motion corrected compressed sensing for free-breathing dynamic cardiac MRI. Magn Reson Med. 2013; 70(2):504–516. [PubMed: 22899104]
24. Jin J, Liu F, Crozier S. Image registration guided, sparsity constrained reconstructions for dynamic MRI. Magn Reson Imaging. 2014; 32(10):1403–1417. [PubMed: 25131631]
25. Chandarana H, Feng L, Ream J, et al. Respiratory Motion-Resolved Compressed Sensing Reconstruction of Free-Breathing Radial Acquisition for Dynamic Liver Magnetic Resonance Imaging. Invest Radiol. 2015; 50(11):749–756. [PubMed: 26146869]
26. Feng L, Axel L, Chandarana H, et al. XD-GRASP: Golden-angle radial MRI with reconstruction of extra motion-state dimensions using compressed sensing. Magn Reson Med. Mar.2015
27. Murphy M, Alley M, Demmel J, et al. Fast l_1-SPIRiT compressed sensing parallel imaging MRI: scalable parallel implementation and clinically feasible runtime. IEEE Trans Med Imaging. 2012; 31(6):1250–1262. [PubMed: 22345529]
28. Lustig, M.; Santos, J.; Donoho, D., et al. k-t SPARSE: high frame rate dynamic MRI exploiting spatio-temporal sparsity. Proc 14th Annu Meet ISMRM; Seattle. 2006; p. 2420
29. Liang ZP, Lauterbur PC. An efficient method for dynamic magnetic resonance imaging. IEEE Trans Med Imaging. 1994; 13(4):677–686. [PubMed: 18218546]
30. Mistretta CA, Wieben O, Velikina J, et al. Highly constrained backprojection for time-resolved MRI. Magn Reson Med. 2006; 55(1):30–40. [PubMed: 16342275]
31. Liang Z-P, Madore B, Glover GH, et al. Fast algorithms for GS-model-based image reconstruction in data-sharing Fourier imaging. IEEE Trans Med Imaging. 2003; 22(8):1026–1030. [PubMed: 12906256]
32. Riederer SJ, Tasciyan T, Farzaneh F, et al. MR fluoroscopy: technical feasibility. Magn Reson Med. 1988; 8(1):1–15. [PubMed: 3173063]
33. van Vaals JJ, Brummer ME, Dixon WT, et al. "Keyhole" method for accelerating imaging of contrast agent uptake. J Magn Reson Imaging. 3(4):671–675. [PubMed: 8347963]

34. Doyle M, Walsh EG, Blackwell GG, et al. Block regional interpolation scheme for k-space (BRISK): a rapid cardiac imaging technique. Magn Reson Med. 1995; 33(2):163–170. [PubMed: 7707905]
35. Korosec FR, Frayne R, Grist TM, et al. Time-resolved contrast-enhanced 3D MR angiography. Magn Reson Med. 1996; 36(3):345–351. [PubMed: 8875403]
36. Lim RP, Shapiro M, Wang EY, et al. 3D time-resolved MR angiography (MRA) of the carotid arteries with time-resolved imaging with stochastic trajectories: comparison with 3D contrast-enhanced Bolus-Chase MRA and 3D time-of-flight MRA. AJNR Am J Neuroradiol. 2008; 29(10): 1847–1854. [PubMed: 18768727]
37. Ma H, Yang J, Liu J, et al. Myocardial perfusion magnetic resonance imaging using sliding-window conjugate-gradient highly constrained back-projection reconstruction for detection of coronary artery disease. Am J Cardiol. 2012; 109(8):1137–1141. [PubMed: 22264595]
38. Ge L, Kino A, Griswold M, et al. Myocardial perfusion MRI with sliding-window conjugate-gradient HYPR. Magn Reson Med. 2009; 62(4):835–839. [PubMed: 19672941]
39. Wang K, Du J, O'Halloran R, et al. Ultrashort TE spectroscopic imaging (UTESI) using complex highly-constrained backprojection with local reconstruction (HYPR LR). Magn Reson Med. 2009; 62(1):127–134. [PubMed: 19353656]
40. Wang K, Schiebler ML, Francois CJ, et al. Pulmonary perfusion MRI using interleaved variable density sampling and HighlY constrained cartesian reconstruction (HYCR). J Magn Reson Imaging. 2013; 38(3):751–756. [PubMed: 23349079]
41. Johnson KM, Velikina J, Wu Y, et al. Improved waveform fidelity using local HYPR reconstruction (HYPR LR). Magn Reson Med. 2008; 59(3):456–462. [PubMed: 18306397]
42. O'Halloran RL, Wen Z, Holmes JH, et al. Iterative projection reconstruction of time-resolved images using highly-constrained back-projection (HYPR). Magn Reson Med. 2008; 59(1):132–139. [PubMed: 18058939]
43. Wu Y, Kim N, Korosec FR, et al. 3D time-resolved contrast-enhanced cerebrovascular MR angiography with subsecond frame update times using radial k-space trajectories and highly constrained projection reconstruction. AJNR Am J Neuroradiol. 28(10):2001–2004. [PubMed: 17928376]
44. Velikina JV, Johnson KM, Wu Y, et al. PC HYPR flow: a technique for rapid imaging of contrast dynamics. J Magn Reson Imaging. 2010; 31(2):447–456. [PubMed: 20099362]
45. Webb AG, Liang ZP, Magin RL, et al. Applications of reduced-encoding MR imaging with generalized-series reconstruction (RIGR). J Magn Reson Imaging. 3(6):925–928. [PubMed: 8280985]
46. Xiang Q-S, Henkelman RM. K-space description for MR imaging of dynamic objects. Magn Reson Med. 1993; 29(3):422–428. [PubMed: 8383792]
47. Jung H, Sung K, Nayak KS, et al. k-t FOCUSS: a general compressed sensing framework for high resolution dynamic MRI. Magn Reson Med. 2009; 61(1):103–116. [PubMed: 19097216]
48. Madore B, Glover GH, Pelc NJ. Unaliasing by fourier-encoding the overlaps using the temporal dimension (UNFOLD), applied to cardiac imaging and fMRI. Magn Reson Med. 1999; 42(5):813–828. [PubMed: 10542340]
49. Brummer ME, Moratal-Pérez D, Hong C-Y, et al. Noquist: reduced field-of-view imaging by direct Fourier inversion. Magn Reson Med. 2004; 51(2):331–342. [PubMed: 14755659]
50. Tsao J, Boesiger P, Pruessmann KP. k-t BLAST and k-t SENSE: dynamic MRI with high frame rate exploiting spatiotemporal correlations. Magn Reson Med. 2003; 50(5):1031–1042. [PubMed: 14587014]
51. Tsao J, Kozerke S. MRI temporal acceleration techniques. J Magn Reson Imaging. 2012; 36(3): 543–560. [PubMed: 22903655]
52. Malik SJ, Schmitz S, O'Regan D, et al. x-f Choice: reconstruction of undersampled dynamic MRI by data-driven alias rejection applied to contrast-enhanced angiography. Magn Reson Med. 2006; 56(4):811–823. [PubMed: 16897770]
53. Pedersen H, Kozerke S, Ringgaard S, et al. k-t PCA: temporally constrained k-t BLAST reconstruction using principal component analysis. Magn Reson Med. 2009; 62(3):706–716. [PubMed: 19585603]

54. Liang D, DiBella EVR, Chen R-R, et al. k-t ISD: dynamic cardiac MR imaging using compressed sensing with iterative support detection. Magn Reson Med. 2012; 68(1):41–53. [PubMed: 22113706]
55. Doneva M, Börnert P, Eggers H, et al. Compressed sensing reconstruction for magnetic resonance parameter mapping. Magn Reson Med. 2010; 64(4):1114–1120. [PubMed: 20564599]
56. Block KT, Uecker M, Frahm J. Model-Based Iterative Reconstruction for Radial Fast Spin-Echo MRI. IEEE Trans Med Imaging. 2009; 28(11):1759–1769. [PubMed: 19502124]
57. Lingala SG, Jacob M. Blind compressive sensing dynamic MRI. IEEE Trans Med Imaging. 2013; 32(6):1132–1145. [PubMed: 23542951]
58. Yoon H, Kim KS, Kim D, et al. Motion adaptive patch-based low-rank approach for compressed sensing cardiac cine MRI. IEEE Trans Med Imaging. 2014; 33(11):2069–2085. [PubMed: 24951686]
59. Ravishankar S, Bresler Y. MR image reconstruction from highly undersampled k-space data by dictionary learning. IEEE Trans Med Imaging. 2011; 30(5):1028–1041. [PubMed: 21047708]
60. Li W, Griswold M, Yu X. Fast cardiac T1 mapping in mice using a model-based compressed sensing method. Magn Reson Med. 2012; 68(4):1127–1134. [PubMed: 22161952]
61. Huang Y, Paisley J, Lin Q, et al. Bayesian nonparametric dictionary learning for compressed sensing MRI. IEEE Trans Image Process. 2014; 23(12):5007–5019. [PubMed: 25265609]
62. McClymont D, Teh I, Whittington HJ, et al. Prospective acceleration of diffusion tensor imaging with compressed sensing using adaptive dictionaries. Magn Reson Med. Aug.2015
63. Tran-Gia J, Stäb D, Wech T, et al. Model-based Acceleration of Parameter mapping (MAP) for saturation prepared radially acquired data. Magn Reson Med. 2013; 70(6):1524–1534. [PubMed: 23315831]
64. Ma D, Gulani V, Seiberlich N, et al. Magnetic resonance fingerprinting. Nature. 2013; 495(7440): 187–192. [PubMed: 23486058]
65. Sumpf TJ, Petrovic A, Uecker M, et al. Fast T2 mapping with improved accuracy using undersampled spin-echo MRI and model-based reconstructions with a generating function. IEEE Trans Med Imaging. 2014; 33(12):2213–2222. [PubMed: 24988592]
66. Velikina JV, Samsonov AA. Reconstruction of dynamic image series from undersampled MRI data using data-driven model consistency condition (MOCCO). Magn Reson Med. 2015; 74(5):1279–1290. [PubMed: 25399724]
67. Prieto C, Usman M, Wild JM, et al. Group sparse reconstruction using intensity-based clustering. Magn Reson Med. 2013; 69(4):1169–1179. [PubMed: 22648740]
68. Majumdar A, Ward RK. Accelerating multi-echo T2 weighted MR imaging: analysis prior group-sparse optimization. J Magn Reson. 2011; 210(1):90–97. [PubMed: 21388848]
69. Usman M, Prieto C, Schaeffter T, et al. k-t Group sparse: a method for accelerating dynamic MRI. Magn Reson Med. 2011; 66(4):1163–1176. [PubMed: 21394781]
70. Adluru G, Tasdizen T, Schabel MC, et al. Reconstruction of 3D dynamic contrast-enhanced magnetic resonance imaging using nonlocal means. J Magn Reson Imaging. 2010; 32(5):1217–1227. [PubMed: 21031528]
71. Akçakaya M, Basha TA, Goddu B, et al. Low-dimensional-structure self-learning and thresholding: regularization beyond compressed sensing for MRI reconstruction. Magn Reson Med. 2011; 66(3): 756–767. [PubMed: 21465542]
72. Wang Y, Ying L. Compressed sensing dynamic cardiac cine MRI using learned spatiotemporal dictionary. IEEE Trans Biomed Eng. 2014; 61(4):1109–1120. [PubMed: 24658236]
73. Song Y, Zhu Z, Lu Y, et al. Reconstruction of magnetic resonance imaging by three-dimensional dual-dictionary learning. Magn Reson Med. 2014; 71(3):1285–1298. [PubMed: 23554046]
74. Cooper MA, Nguyen TD, Xu B, et al. Patch based reconstruction of undersampled data (PROUD) for high signal-to-noise ratio and high frame rate contrast enhanced liver imaging. Magn Reson Med. 2015; 74(6):1587–1597. [PubMed: 25483782]
75. Mistretta CA. Sub-Nyquist acquisition and constrained reconstruction in time resolved angiography. Med Phys. 2011; 38(6):2975–2985. [PubMed: 21815371]

76. Liu J, Saloner D. Accelerated MRI with CIRcular Cartesian UnderSampling (CIRCUS): a variable density Cartesian sampling strategy for compressed sensing and parallel imaging. Quant Imaging Med Surg. 2014; 4(1):57–67. [PubMed: 24649436]
77. Ahmad R, Xue H, Giri S, et al. Variable density incoherent spatiotemporal acquisition (VISTA) for highly accelerated cardiac MRI. Magn Reson Med. 2015; 74(5):1266–1278. [PubMed: 25385540]
78. Block KT, Uecker M, Frahm J. Undersampled radial MRI with multiple coils. Iterative image reconstruction using a total variation constraint. Magn Reson Med. 2007; 57(6):1086–1098. [PubMed: 17534903]
79. Chandarana H, Feng L, Block TK, et al. Free-breathing contrast-enhanced multiphase MRI of the liver using a combination of compressed sensing, parallel imaging, and golden-angle radial sampling. Invest Radiol. 2013; 48(1):10–16. [PubMed: 23192165]
80. Chatnuntawech I, Gagoski B, Bilgic B, et al. Accelerated (1) H MRSI using randomly undersampled spiral-based k-space trajectories. Magn Reson Med. Jul.2014
81. Holland DJ, Liu C, Song X, et al. Compressed sensing reconstruction improves sensitivity of variable density spiral fMRI. Magn Reson Med. 2013; 70(6):1634–1643. [PubMed: 23390043]
82. Li Y, Yang R, Zhang C, et al. Analysis of generalized rosette trajectory for compressed sensing MRI. Med Phys. 2015; 42(9):5530–5544. [PubMed: 26329000]
83. Haldar JP, Hernando D, Liang Z-P. Compressed-sensing MRI with random encoding. IEEE Trans Med Imaging. 2011; 30(4):893–903. [PubMed: 20937579]
84. Barger AV, Block WF, Toropov Y, et al. Time-resolved contrast-enhanced imaging with isotropic resolution and broad coverage using an undersampled 3D projection trajectory. Magn Reson Med. 2002; 48(2):297–305. [PubMed: 12210938]
85. Addy NO, Ingle RR, Wu HH, et al. High-resolution variable-density 3D cones coronary MRA. Magn Reson Med. 2015; 74(3):614–621. [PubMed: 26172829]
86. Raja R, Sinha N. Adaptive k-space sampling design for edge-enhanced DCE-MRI using compressed sensing. Magn Reson Imaging. 2014; 32(7):899–912. DOI: 10.1016/j.mri.2013.12.022 [PubMed: 24848294]
87. Seeger M, Nickisch H, Pohmann R, et al. Optimization of k-space trajectories for compressed sensing by Bayesian experimental design. Magn Reson Med. 2010; 63(1):116–126. [PubMed: 19859957]
88. Zhang T, Pauly JM, Levesque IR. Accelerating parameter mapping with a locally low rank constraint. Magn Reson Med. 2015; 73(2):655–661. [PubMed: 24500817]
89. Hutter J, Schmitt P, Aandal G, et al. Low-rank and sparse matrix decomposition for compressed sensing reconstruction of magnetic resonance 4D phase contrast blood flow imaging (loSDeCoS 4D-PCI). Med Image Comput Comput Assist Interv. 2013; 16(Pt 1):558–565. [PubMed: 24505711]
90. Otazo R, Candès E, Sodickson DK. Low-rank plus sparse matrix decomposition for accelerated dynamic MRI with separation of background and dynamic components. Magn Reson Med. 2014; 00:1–12. DOI: 10.1002/mrm.25240
91. Majumdar A, Ward RK. Exploiting rank deficiency and transform domain sparsity for MR image reconstruction. Magn Reson Imaging. 2012; 30(1):9–18. [PubMed: 21937179]
92. Hollingsworth KG. Reducing acquisition time in clinical MRI by data undersampling and compressed sensing reconstruction. Phys Med Biol. 2015; 60(21):R297–R322. [PubMed: 26448064]
93. Jaspan ON, Fleysher R, Lipton ML. Compressed sensing MRI: a review of the clinical literature. Br J Radiol. Oct.2015 :20150487. [PubMed: 26402216]
94. Wu B, Li W, Guidon A, et al. Whole brain susceptibility mapping using compressed sensing. Magn Reson Med. 2012; 67(1):137–147. [PubMed: 21671269]
95. Wiens CN, McCurdy CM, Willig-Onwuachi JD, et al. R2*-corrected water-fat imaging using compressed sensing and parallel imaging. Magn Reson Med. 2014; 71(2):608–616. [PubMed: 23475787]
96. Doneva M, Börnert P, Eggers H, et al. Compressed sensing for chemical shift-based water-fat separation. Magn Reson Med. 2010; 64(6):1749–1759. [PubMed: 20859998]

97. Sharma SD, Hu HH, Nayak KS. Accelerated water-fat imaging using restricted subspace field map estimation and compressed sensing. Magn Reson Med. 2012; 67(3):650–659. [PubMed: 21713983]

98. Sharma SD, Hu HH, Nayak KS. Chemical shift encoded water-fat separation using parallel imaging and compressed sensing. Magn Reson Med. 2013; 69(2):456–466. [PubMed: 22505285]

99. Rapacchi S, Han F, Natsuaki Y, et al. High spatial and temporal resolution dynamic contrast-enhanced magnetic resonance angiography using compressed sensing with magnitude image subtraction. Magn Reson Med. 2014; 71(5):1771–1783. [PubMed: 23801456]

100. Cukur T, Lustig M, Nishimura DG. Improving non-contrast-enhanced steady-state free precession angiography with compressed sensing. Magn Reson Med. 2009; 61(5):1122–1131. [PubMed: 19230013]

101. Dautry R, Edjlali M, Roca P, et al. Interest of HYPR flow dynamic MRA for characterization of cerebral arteriovenous malformations: comparison with TRICKS MRA and catheter DSA. Eur Radiol. 2015; 25(11):3230–3237. [PubMed: 25916388]

102. Stalder AF, Schmidt M, Quick HH, et al. Highly undersampled contrast-enhanced MRA with iterative reconstruction: Integration in a clinical setting. Magn Reson Med. Dec.2014

103. Li B, Dong L, Chen B, et al. Turbo fast three-dimensional carotid artery black-blood MRI by combining three-dimensional MERGE sequence with compressed sensing. Magn Reson Med. 2013; 70(5):1347–1352. [PubMed: 23280949]

104. Tao Y, Rilling G, Davies M, et al. Carotid blood flow measurement accelerated by compressed sensing: validation in healthy volunteers. Magn Reson Imaging. 2013; 31(9):1485–1491. [PubMed: 23830111]

105. Akçakaya M, Hu P, Chuang ML, et al. Accelerated noncontrast-enhanced pulmonary vein MRA with distributed compressed sensing. J Magn Reson Imaging. 2011; 33(5):1248–1255. [PubMed: 21509886]

106. Koktzoglou I, Mistretta CA, Giri S, et al. Simultaneous static and cine nonenhanced MR angiography using radial sampling and highly constrained back projection reconstruction. Magn Reson Med. 2014; 72(4):1079–1086. [PubMed: 24407879]

107. Forman C, Grimm R, Hutter JM, et al. Free-breathing whole-heart coronary MRA: motion compensation integrated into 3D cartesian compressed sensing reconstruction. Med Image Comput Comput Assist Interv. 2013; 16(Pt 2):575–582. [PubMed: 24579187]

108. Prieto C, Doneva M, Usman M, et al. Highly efficient respiratory motion compensated free-breathing coronary MRA using golden-step Cartesian acquisition. J Magn Reson Imaging. 2015; 41(3):738–746. [PubMed: 24573992]

109. Akçakaya M, Basha TA, Chan RH, et al. Accelerated isotropic sub-millimeter whole-heart coronary MRI: compressed sensing versus parallel imaging. Magn Reson Med. 2014; 71(2):815–822. [PubMed: 23440946]

110. Zhang T, Yousaf U, Hsiao A, et al. Clinical performance of a free-breathing spatiotemporally accelerated 3-D time-resolved contrast-enhanced pediatric abdominal MR angiography. Pediatr Radiol. 2015; 45(11):1635–1643. [PubMed: 26040509]

111. Basha TA, Akçakaya M, Goddu B, et al. Accelerated three-dimensional cine phase contrast imaging using randomly undersampled echo planar imaging with compressed sensing reconstruction. NMR Biomed. 2015; 28(1):30–39. [PubMed: 25323208]

112. Hsiao A, Lustig M, Alley MT, et al. Rapid pediatric cardiac assessment of flow and ventricular volume with compressed sensing parallel imaging volumetric cine phase-contrast MRI. AJR Am J Roentgenol. 2012; 198(3):W250–W259. [PubMed: 22358022]

113. Hsiao A, Lustig M, Alley MT, et al. Evaluation of valvular insufficiency and shunts with parallel-imaging compressed-sensing 4D phase-contrast MR imaging with stereoscopic 3D velocity-fusion volume-rendered visualization. Radiology. 2012; 265(1):87–95. [PubMed: 22923717]

114. Tariq U, Hsiao A, Alley M, et al. Venous and arterial flow quantification are equally accurate and precise with parallel imaging compressed sensing 4D phase contrast MRI. J Magn Reson Imaging. 2013; 37(6):1419–1426. [PubMed: 23172846]

115. Giese D, Wong J, Greil GF, et al. Towards highly accelerated Cartesian time-resolved 3D flow cardiovascular magnetic resonance in the clinical setting. J Cardiovasc Magn Reson. 2014; 16:42. [PubMed: 24942253]

116. Hsiao A, Yousaf U, Alley MT, et al. Improved quantification and mapping of anomalous pulmonary venous flow with four-dimensional phase-contrast MRI and interactive streamline rendering. J Magn Reson Imaging. Apr.2015

117. Kim D, Dyvorne HA, Otazo R, et al. Accelerated phase-contrast cine MRI using k-t SPARSE-SENSE. Magn Reson Med. 2012; 67(4):1054–1064. [PubMed: 22083998]

118. Dyvorne H, Knight-Greenfield A, Jajamovich G, et al. Abdominal 4D flow MR imaging in a breath hold: combination of spiral sampling and dynamic compressed sensing for highly accelerated acquisition. Radiology. 2015; 275(1):245–254. [PubMed: 25325326]

119. Hutter J, Schmitt P, Saake M, et al. Multi-dimensional flow-preserving compressed sensing (MuFloCoS) for time-resolved velocity-encoded phase contrast MRI. IEEE Trans Med Imaging. 2015; 34(2):400–414. [PubMed: 25252278]

120. Jung H, Park J, Yoo J, et al. Radial k-t FOCUSS for high-resolution cardiac cine MRI. Magn Reson Med. 2010; 63(1):68–78. [PubMed: 19859952]

121. Tsao J, Kozerke S, Boesiger P, et al. Optimizing spatiotemporal sampling for k-t BLAST and k-t SENSE: application to high-resolution real-time cardiac steady-state free precession. Magn Reson Med. 2005; 53(6):1372–1382. [PubMed: 15906282]

122. Feng L, Srichai MB, Lim RP, et al. Highly accelerated real-time cardiac cine MRI using k-t SPARSE-SENSE. Magn Reson Med. 2013; 70(1):64–74. [PubMed: 22887290]

123. Paul J, Divkovic E, Wundrak S, et al. High-resolution respiratory self-gated golden angle cardiac MRI: Comparison of self-gating methods in combination with k-t SPARSE SENSE. Magn Reson Med. 2015; 73(1):292–298. [PubMed: 24478142]

124. Usman M, Atkinson D, Heathfield E, et al. Whole left ventricular functional assessment from two minutes free breathing multi-slice CINE acquisition. Phys Med Biol. 2015; 60(7):N93–N107. [PubMed: 25768044]

125. Wech T, Pickl W, Tran-Gia J, et al. Whole-heart cine MRI in a single breath-hold--a compressed sensing accelerated 3D acquisition technique for assessment of cardiac function. Rofo. 2014; 186(1):37–41. [PubMed: 23996623]

126. Vincenti G, Monney P, Chaptinel J, et al. Compressed sensing single-breath-hold CMR for fast quantification of LV function, volumes, and mass. JACC Cardiovasc Imaging. 2014; 7(9):882–892. [PubMed: 25129517]

127. Nam S, Hong SN, Akçakaya M, et al. Compressed sensing reconstruction for undersampled breath-hold radial cine imaging with auxiliary free-breathing data. J Magn Reson Imaging. 2014; 39(1):179–188. [PubMed: 23857797]

128. Adluru G, Awate SP, Tasdizen T, et al. Temporally constrained reconstruction of dynamic cardiac perfusion MRI. Magn Reson Med. 2007; 57(6):1027–1036. [PubMed: 17534924]

129. Plein S, Kozerke S, Suerder D, et al. High spatial resolution myocardial perfusion cardiac magnetic resonance for the detection of coronary artery disease. Eur Heart J. 2008; 29(17):2148–2155. [PubMed: 18641047]

130. Manka R, Vitanis V, Boesiger P, et al. Clinical feasibility of accelerated, high spatial resolution myocardial perfusion imaging. JACC Cardiovasc Imaging. 2010; 3(7):710–717. [PubMed: 20633848]

131. Lingala SG, DiBella E, Adluru G, et al. Accelerating free breathing myocardial perfusion MRI using multi coil radial k-t SLR. Phys Med Biol. 2013; 58(20):7309–7327. [PubMed: 24077063]

132. Sharif B, Arsanjani R, Dharmakumar R, et al. All-systolic non-ECG-gated myocardial perfusion MRI: Feasibility of multi-slice continuous first-pass imaging. Magn Reson Med. Jun.2015

133. Harrison A, Adluru G, Damal K, et al. Rapid ungated myocardial perfusion cardiovascular magnetic resonance: preliminary diagnostic accuracy. J Cardiovasc Magn Reson. 2013; 15:26. [PubMed: 23537093]

134. Xu J, Kim D, Otazo R, et al. Towards a five-minute comprehensive cardiac MR examination using highly accelerated parallel imaging with a 32-element coil array: feasibility and initial comparative evaluation. J Magn Reson Imaging. 2013; 38(1):180–188. [PubMed: 23197471]

135. Stäb D, Wech T, Breuer FA, et al. High resolution myocardial first-pass perfusion imaging with extended anatomic coverage. J Magn Reson Imaging. 2014; 39(6):1575–1587. [PubMed: 24151153]
136. Adluru G, Chen L, Kim S-E, et al. Three-dimensional late gadolinium enhancement imaging of the left atrium with a hybrid radial acquisition and compressed sensing. J Magn Reson Imaging. 2011; 34(6):1465–1471. [PubMed: 21972108]
137. Akçakaya M, Rayatzadeh H, Basha TA, et al. Accelerated late gadolinium enhancement cardiac MR imaging with isotropic spatial resolution using compressed sensing: initial experience. Radiology. 2012; 264(3):691–699. [PubMed: 22820734]
138. Weingärtner S, Akçakaya M, Roujol S, et al. Free-breathing combined three-dimensional phase sensitive late gadolinium enhancement and T1 mapping for myocardial tissue characterization. Magn Reson Med. 2015; 74(4):1032–1041. [PubMed: 25324205]
139. Zhang T, Chowdhury S, Lustig M, et al. Clinical performance of contrast enhanced abdominal pediatric MRI with fast combined parallel imaging compressed sensing reconstruction. J Magn Reson Imaging. 2014; 40(1):13–25. [PubMed: 24127123]
140. Vasanawala SS, Alley MT, Hargreaves BA, et al. Improved pediatric MR imaging with compressed sensing. Radiology. 2010; 256(2):607–616. [PubMed: 20529991]
141. Chen B, Zhao K, Li B, et al. High temporal resolution dynamic contrast-enhanced MRI using compressed sensing-combined sequence in quantitative renal perfusion measurement. Magn Reson Imaging. 2015; 33(8):962–969. [PubMed: 25967586]
142. Chandarana H, Block TK, Ream J, et al. Estimating liver perfusion from free-breathing continuously acquired dynamic gadolinium-ethoxybenzyl-diethylenetriamine pentaacetic acid-enhanced acquisition with compressed sensing reconstruction. Invest Radiol. 2015; 50(2):88–94. [PubMed: 25333309]
143. Ream JM, Doshi A, Lala SV, et al. High Spatiotemporal Resolution Dynamic Contrast-Enhanced MR Enterography in Crohn Disease Terminal Ileitis Using Continuous Golden-Angle Radial Sampling, Compressed Sensing, and Parallel Imaging. AJR Am J Roentgenol. 2015; 204(6):W663–W669. [PubMed: 26001254]
144. Rosenkrantz AB, Geppert C, Grimm R, et al. Dynamic contrast-enhanced MRI of the prostate with high spatiotemporal resolution using compressed sensing, parallel imaging, and continuous golden-angle radial sampling: preliminary experience. J Magn Reson Imaging. 2015; 41(5): 1365–1373. [PubMed: 24833417]
145. Bilgic B, Gagoski B, Kok T, et al. Lipid suppression in CSI with spatial priors and highly undersampled peripheral k-space. Magn Reson Med. 2013; 69(6):1501–1511. [PubMed: 22807147]
146. Sharma SD, Hu HH, Nayak KS. Accelerated T2*-compensated fat fraction quantification using a joint parallel imaging and compressed sensing framework. J Magn Reson Imaging. 2013; 38(5): 1267–1275. [PubMed: 23390111]
147. Mann LW, Higgins DM, Peters CN, et al. Accelerating MR Imaging Liver Steatosis Measurement Using Combined Compressed Sensing and Parallel Imaging: A Quantitative Evaluation. Radiology. Jul.2015 :150320.
148. Chen Y, Jiang Y, Pahwa S, et al. MR Fingerprinting for Rapid Quantitative Abdominal Imaging. Radiology. Jan.2016 :152037.
149. Nagarajan R, Iqbal Z, Burns B, et al. Accelerated echo planar J-resolved spectroscopic imaging in prostate cancer: a pilot validation of non-linear reconstruction using total variation and maximum entropy. NMR Biomed. 2015; 28(11):1366–1373. [PubMed: 26346702]
150. Zhao L, Fielden SW, Feng X, et al. Rapid 3D dynamic arterial spin labeling with a sparse model-based image reconstruction. Neuroimage. 2015; 121:205–216. [PubMed: 26169322]
151. Lebel RM, Jones J, Ferre J-C, et al. Highly accelerated dynamic contrast enhanced imaging. Magn Reson Med. 2014; 71(2):635–644. [PubMed: 23504992]
152. Rossi Espagnet MC, Bangiyev L, Haber M, et al. High-Resolution DCE-MRI of the Pituitary Gland Using Radial k-Space Acquisition with Compressed Sensing Reconstruction. AJNR Am J Neuroradiol. 2015; 36(8):1444–1449. [PubMed: 25953760]

153. Wilson NE, Iqbal Z, Burns BL, et al. Accelerated five-dimensional echo planar J-resolved spectroscopic imaging: Implementation and pilot validation in human brain. Magn Reson Med. 2016; 75(1):42–51. [PubMed: 25599891]

154. Sarma MK, Nagarajan R, Macey PM, et al. Accelerated echo-planar J-resolved spectroscopic imaging in the human brain using compressed sensing: a pilot validation in obstructive sleep apnea. AJNR Am J Neuroradiol. 2014; 35(6 Suppl):S81–S89. [PubMed: 24503554]

155. Badve C, Yu A, Rogers M, et al. Simultaneous T1 and T2 Brain Relaxometry in Asymptomatic Volunteers using Magnetic Resonance Fingerprinting. Tomography. 2015

156. Chavarrías C, Abascal JFPJ, Montesinos P, et al. Exploitation of temporal redundancy in compressed sensing reconstruction of fMRI studies with a prior-based algorithm (PICCS). Med Phys. 2015; 42(7):3814–3821. [PubMed: 26133583]

157. Nguyen HM, Glover GH. A modified generalized series approach: application to sparsely sampled FMRI. IEEE Trans Biomed Eng. 2013; 60(10):2867–2877. [PubMed: 23744655]

158. Cheng J, Shen D, Basser PJ, et al. Joint 6D k-q Space Compressed Sensing for Accelerated High Angular Resolution Diffusion MRI. Inf Process Med Imaging. 2015; 24:782–793. [PubMed: 26221718]

159. Ning L, Setsompop K, Michailovich O, et al. A joint compressed-sensing and super-resolution approach for very high-resolution diffusion imaging. Neuroimage. 2015; 125:386–400. [PubMed: 26505296]

160. Landman BA, Bogovic JA, Wan H, et al. Resolution of crossing fibers with constrained compressed sensing using diffusion tensor MRI. Neuroimage. 2012; 59(3):2175–2186. [PubMed: 22019877]

161. Michailovich O, Rathi Y, Dolui S. Spatially regularized compressed sensing for high angular resolution diffusion imaging. IEEE Trans Med Imaging. 2011; 30(5):1100–1115. [PubMed: 21536524]

162. Kuhnt D, Bauer MHA, Egger J, et al. Fiber tractography based on diffusion tensor imaging compared with high-angular-resolution diffusion imaging with compressed sensing: initial experience. Neurosurgery. 2013; 72(Suppl 1):165–175. [PubMed: 23254805]

163. Wang Y-XJ, Lo GG, Yuan J, et al. Magnetic resonance imaging for lung cancer screen. J Thorac Dis. 6(9):1340–1348. [PubMed: 25276380]

164. Ajraoui S, Lee KJ, Deppe MH, et al. Compressed sensing in hyperpolarized 3He lung MRI. Magn Reson Med. 2010; 63(4):1059–1069. [PubMed: 20373407]

165. Tahir BA, Van Holsbeke C, Ireland RH, et al. Comparison of CT-based Lobar Ventilation with (3)He MR Imaging Ventilation Measurements. Radiology. Aug.2015 :142278.

166. Marshall H, Parra-Robles J, Deppe MH, et al. (3)He pO2 mapping is limited by delayed-ventilation and diffusion in chronic obstructive pulmonary disease. Magn Reson Med. 2014; 71(3):1172–1178. [PubMed: 23661570]

167. Ma W, Sheikh K, Svenningsen S, et al. Ultra-short echo-time pulmonary MRI: evaluation and reproducibility in COPD subjects with and without bronchiectasis. J Magn Reson Imaging. 2015; 41(5):1465–1474. [PubMed: 24965907]

168. Worters PW, Sung K, Stevens KJ, et al. Compressed-sensing multispectral imaging of the postoperative spine. J Magn Reson Imaging. 2013; 37(1):243–248. [PubMed: 22791572]

169. Wilson NE, Burns BL, Iqbal Z, et al. Correlated spectroscopic imaging of calf muscle in three spatial dimensions using group sparse reconstruction of undersampled single and multichannel data. Magn Reson Med. 2015; 74(5):1199–1208. [PubMed: 26382049]

170. Madelin G, Chang G, Otazo R, et al. Compressed sensing sodium MRI of cartilage at 7T: preliminary study. J Magn Reson. 2012; 214(1):360–365. [PubMed: 22204825]

171. Pandit P, Rivoire J, King K, et al. Accelerated T1ρ acquisition for knee cartilage quantification using compressed sensing and data-driven parallel imaging: A feasibility study. Magn Reson Med. Apr.2015

172. Zhou Y, Pandit P, Pedoia V, et al. Accelerating t1ρ cartilage imaging using compressed sensing with iterative locally adapted support detection and JSENSE. Magn Reson Med. May.2015

173. Parasoglou P, Feng L, Xia D, et al. Rapid 3D-imaging of phosphocreatine recovery kinetics in the human lower leg muscles with compressed sensing. Magn Reson Med. 2012; 68(6):1738–1746. [PubMed: 23023624]
174. Hollingsworth KG, Higgins DM, McCallum M, et al. Investigating the quantitative fidelity of prospectively undersampled chemical shift imaging in muscular dystrophy with compressed sensing and parallel imaging reconstruction. Magn Reson Med. 2014; 72(6):1610–1619. [PubMed: 24347306]
175. Loughran T, Higgins DM, McCallum M, et al. Improving highly accelerated fat fraction measurements for clinical trials in muscular dystrophy: origin and quantitative effect of R2* changes. Radiology. 2015; 275(2):570–578. [PubMed: 25575118]
176. Smith DS, Welch EB, Li X, et al. Quantitative effects of using compressed sensing in dynamic contrast enhanced MRI. Phys Med Biol. 2011; 56(15):4933–4946. [PubMed: 21772079]
177. Morton G, Ishida M, Schuster A, et al. Perfusion cardiovascular magnetic resonance: Comparison of an advanced, high-resolution and a standard sequence. J Cardiovasc Magn Reson. 2012; 14:34. [PubMed: 22682016]
178. Carlsson M, Töger J, Kanski M, et al. Quantification and visualization of cardiovascular 4D velocity mapping accelerated with parallel imaging or k-t BLAST: head to head comparison and validation at 1.5 T and 3 T. J Cardiovasc Magn Reson. 2011; 13:55. [PubMed: 21970399]
179. Gamper U, Boesiger P, Kozerke S. Compressed sensing in dynamic MRI. Magn Reson Med. 2008; 59(2):365–373. [PubMed: 18228595]
180. Sharma SD, Fong CL, Tzung BS, et al. Clinical image quality assessment of accelerated magnetic resonance neuroimaging using compressed sensing. Invest Radiol. 2013; 48(9):638–645. [PubMed: 23538890]
181. Hong M, Yu Y, Wang H, et al. Compressed sensing MRI with singular value decomposition-based sparsity basis. Phys Med Biol. 2011; 56(19):6311–6325. [PubMed: 21896962]
182. Han S, Paulsen JL, Zhu G, et al. Temporal/spatial resolution improvement of in vivo DCE-MRI with compressed sensing-optimized FLASH. Magn Reson Imaging. 2012; 30(6):741–752. [PubMed: 22465192]
183. Fushimi Y, Fujimoto K, Okada T, et al. Compressed Sensing 3-Dimensional Time-of-Flight Magnetic Resonance Angiography for Cerebral Aneurysms: Optimization and Evaluation. Invest Radiol. Nov.2015
184. Benning M, Gladden L, Holland D, et al. Phase reconstruction from velocity-encoded MRI measurements--a survey of sparsity-promoting variational approaches. J Magn Reson. 2014; 238:26–43. [PubMed: 24291331]
185. Lee GR, Seiberlich N, Sunshine JL, et al. Rapid time-resolved magnetic resonance angiography via a multiecho radial trajectory and GraDeS reconstruction. Magn Reson Med. 2013; 69(2):346–359. [PubMed: 22473742]
186. Khare K, Hardy CJ, King KF, et al. Accelerated MR imaging using compressive sensing with no free parameters. Magn Reson Med. 2012; 68(5):1450–1457. [PubMed: 22266597]
187. Pipe, J. MRI UNBOUND. http://www.ismrm.org/mri_unbound/
188. Fat-Water Separation: Insights, Applications & Progress in MRI. http://www.ismrm.org/workshops/FatWater12/data.htm
189. Daducci A, Canales-Rodríguez EJ, Descoteaux M, et al. Quantitative comparison of reconstruction methods for intra-voxel fiber recovery from diffusion MRI. IEEE Trans Med Imaging. 2014; 33(2):384–399. [PubMed: 24132007]
190. Hansen MS, Sørensen TS. Gadgetron: an open source framework for medical image reconstruction. Magn Reson Med. 2013; 69(6):1768–1776. [PubMed: 22791598]
191. Nam S, Akçakaya M, Basha T, et al. Compressed sensing reconstruction for whole-heart imaging with 3D radial trajectories: a graphics processing unit implementation. Magn Reson Med. 2013; 69(1):91–102. [PubMed: 22392604]
192. Xue H, Inati S, Sørensen TS, et al. Distributed MRI reconstruction using Gadgetron-based cloud computing. Magn Reson Med. 2015; 73(3):1015–1025. [PubMed: 24687458]
193. Chang C-H, Ji J. Compressed sensing MRI with multichannel data using multicore processors. Magn Reson Med. 2010; 64(4):1135–1139. [PubMed: 20564584]

194. Patino M, Fuentes JM, Singh S, et al. Iterative Reconstruction Techniques in Abdominopelvic CT: Technical Concepts and Clinical Implementation. AJR Am J Roentgenol. 2015; 205(1):W19–W31. [PubMed: 26102414]

195. Setsompop K, Gagoski BA, Polimeni JR, et al. Blipped-controlled aliasing in parallel imaging for simultaneous multislice echo planar imaging with reduced g-factor penalty. Magn Reson Med. 2012; 67(5):1210–1224. [PubMed: 21858868]

196. Xu J, Moeller S, Auerbach EJ, et al. Evaluation of slice accelerations using multiband echo planar imaging at 3 T. Neuroimage. 2013; 83:991–1001. [PubMed: 23899722]

197. Wright KL, Harrell MW, Jesberger JA, et al. Clinical evaluation of CAIPIRINHA: comparison against a GRAPPA standard. J Magn Reson Imaging. 2014; 39(1):189–194. [PubMed: 24123420]

198. Breuer FA, Blaimer M, Mueller MF, et al. Controlled aliasing in volumetric parallel imaging (2D CAIPIRINHA). Magn Reson Med. 2006; 55(3):549–556. [PubMed: 16408271]

199. Seiberlich N, Ehses P, Duerk J, et al. Improved radial GRAPPA calibration for real-time free-breathing cardiac imaging. Magn Reson Med. 2011; 65(2):492–505. [PubMed: 20872865]

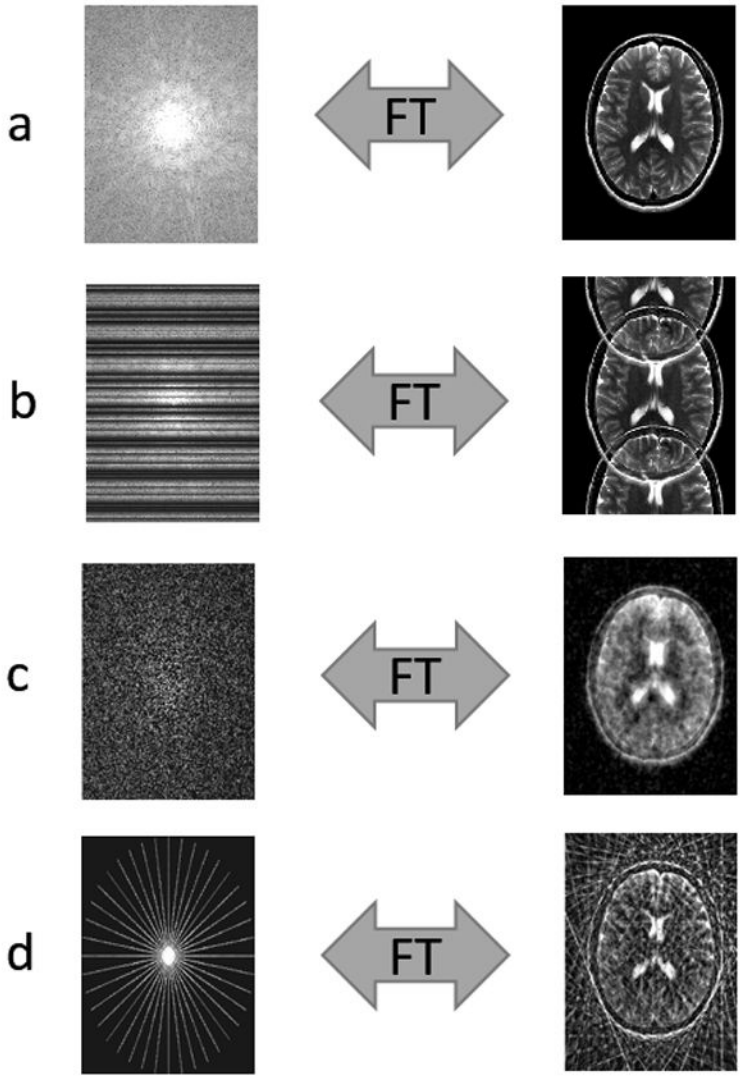

Figure 1.

(a) Fully sampled k-space is converted to an image via the Fourier Transform. (b) Cartesian undersampling by factor of 2, where every other line of k-space is missing. The resulting image is corrupted by aliasing or fold-over artifacts. (c) Random Cartesian undersampling. If k-space points are skipped in such random fashion, the resulting aliasing artifacts no longer appear as distinct replicas of the image (as in (b)), but instead as blurring or noise-like artifacts. This type of sampling is typically not realizable in 2D. (d) Radial undersampling by factor of 9. The resulting image contains streak artifacts due to the undersampling, but the bulk of the image is recognizable since the center of k-space is well sampled.

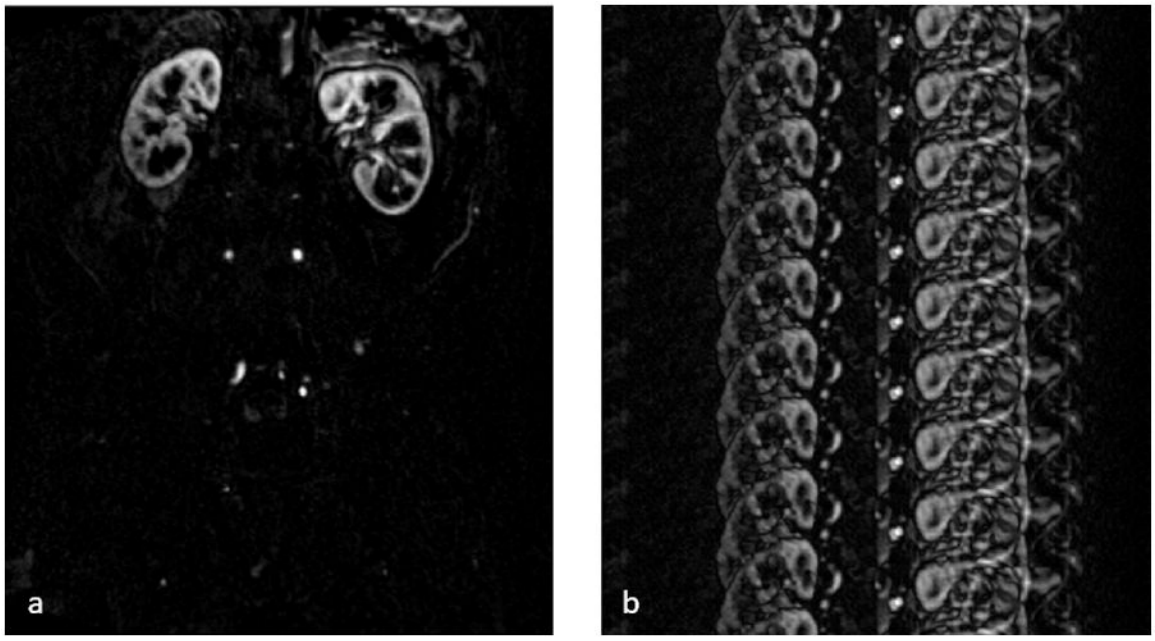

Figure 2.

(a) An example of a sparse MR image, specifically a single partition subtraction image from a 3D abdominal and pelvic contrast enhanced MR angiogram, where few of the image pixels contain signal (and are bright), but most of the image pixels are near zero. (b) When the k-space data are undersampled, the resulting image is no longer sparse due to the presence of aliasing artifacts. If it is known a priori that the image should be sparse, a sparse reconstruction can be used to recover the original image.

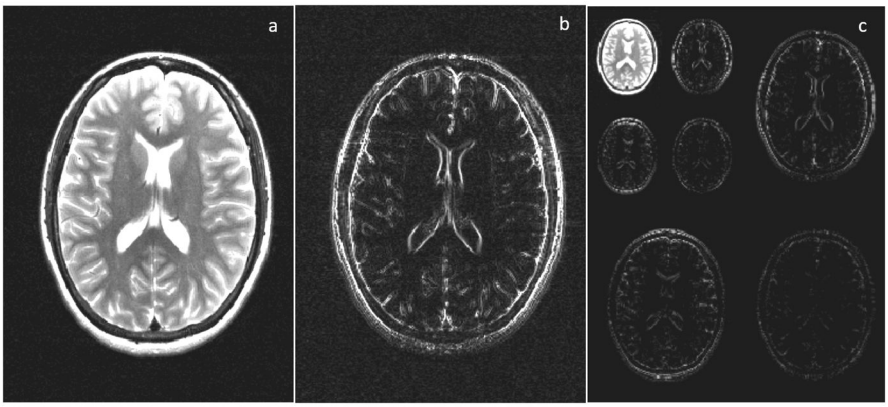

Figure 3.

(a) An axial brain image. (b) Horizontal finite differences transform of the image shown in (a). This transform shows the differences between neighboring pixels, and thus highlights edges in the image. Many images are sparse, i.e. contain more pixels with near-zero values, after such a spatial finite differences transform. (c) Wavelet transform of the image shown in (a), where the transformed images are again sparse compared to the untransformed image (a).

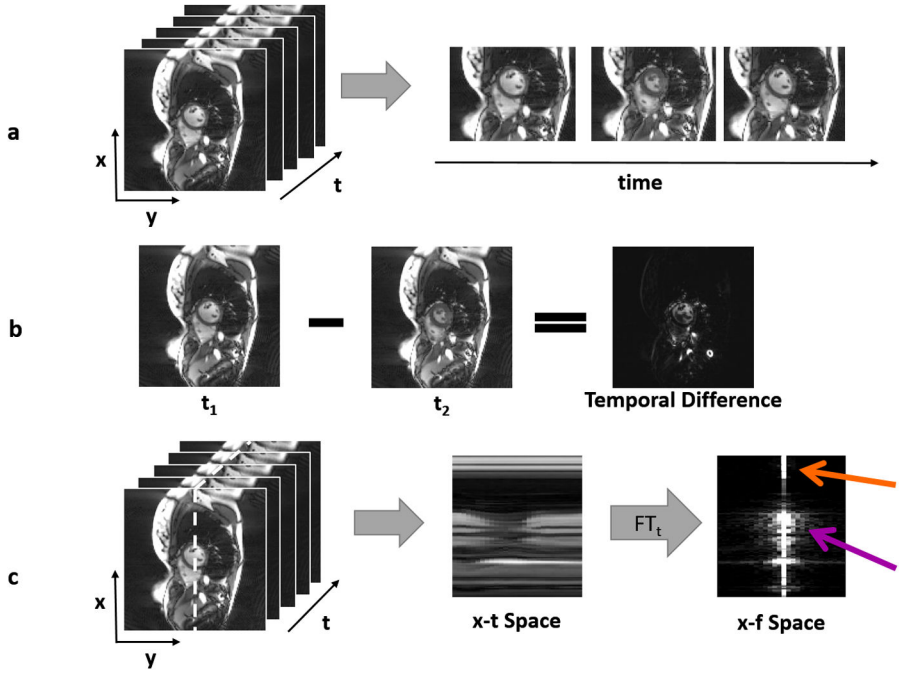

Figure 4.

(a) A time series of dynamic cardiac images is shown, where the x-y plane shows the images, and the t axis depicts the time dimension (left). Three different images of the heart show the motion that occurs through time (right). (b) When one frame from the dynamic dataset is subtracted from another, the result is a sparser image because many tissues are stationary from frame to frame. Only pixels near the heart change, and these are reflected in the temporal difference image. (c) The 3D space-time data can be examined along one slice of the x-t plane (left), designated by the white dotted line. The areas with significant motion can be clearly seen in the "x-t space" image (middle). If a Fourier transform is applied to the x-t space in the time direction, the result is the image representation in the spatiotemporal domain (x-f space, right). Static areas of the image will only have a single bright pixel in the x-f space (orange arrow), and only pixels with significant motion will contribute many non-zero pixels (purple arrow), making x-f space sparse in many dynamic applications.

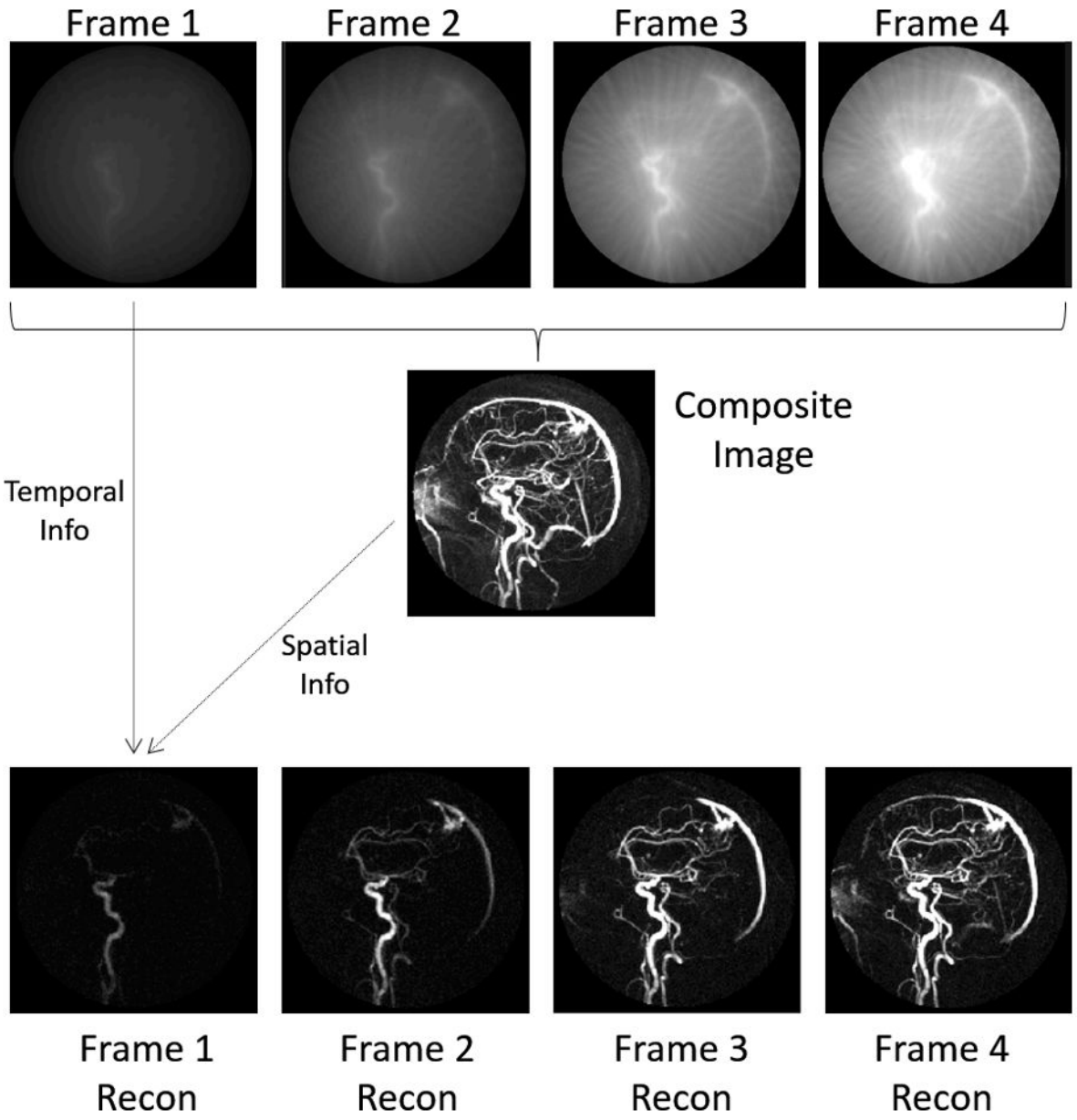

Figure 5.

(top) By sampling data using an undersampled radial scheme, dynamic images of low spatial resolution but high temporal resolution can be collected. These images show the enhancement in different regions over time, but are not usable because of their low resolution. (middle) By gathering all acquired radial projections from each timeframe, a high spatial resolution composite image can be created. This single static image displays all enhanced vessels at a high resolution, but does not show the order in which they enhance. HYPR works by combining spatial information from the high-resolution composite image with temporal information from the low-resolution dynamic images. This reconstruction yields a time series of high spatial and high temporal resolution images (bottom row) that shows dynamic enhancement of the vessels.

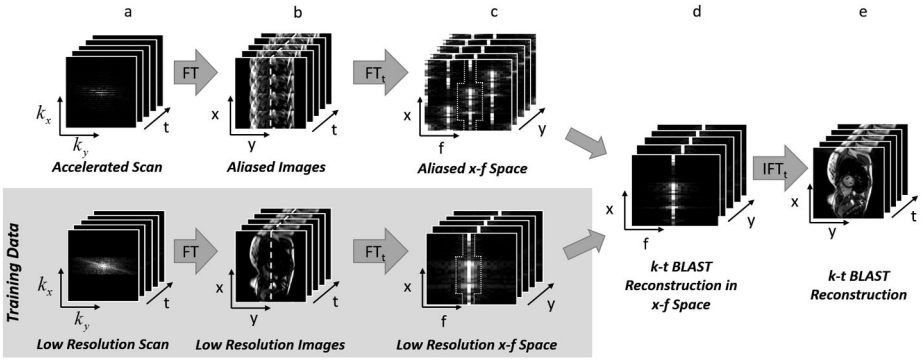

Figure 6.

A schematic of the k-t BLAST reconstruction technique. Both undersampled data with high spatial and temporal resolution (a, top) and fully-sampled low resolution data (a, bottom) are collected. The undersampled accelerated data are used to generate the image, and the low resolution data serve as training data for the k-t BLAST reconstruction. After using Fourier transform to convert the datasets into the image domain (b), the aliasing in the undersampled data can be seen (b, top). By applying a Fourier transform in time, the data are converted to the x-f domain (c). If the undersampled data are collected using the k-t interleaved sampling pattern, the duplicates seen in the x-f domain will be offset in the undersampled data (c, top). However, the low resolution training data do not show aliasing in the x-f domain because they are fully-sampled (c, bottom). A knowledge of the structure of the x-f training data (indicated by the dashed shape in x-f space) can be used to remove aliasing in the high resolution aliased x-f space (d). The final images are generated by applying an inverse Fourier transform to the reconstructed high resolution x-f data (e).

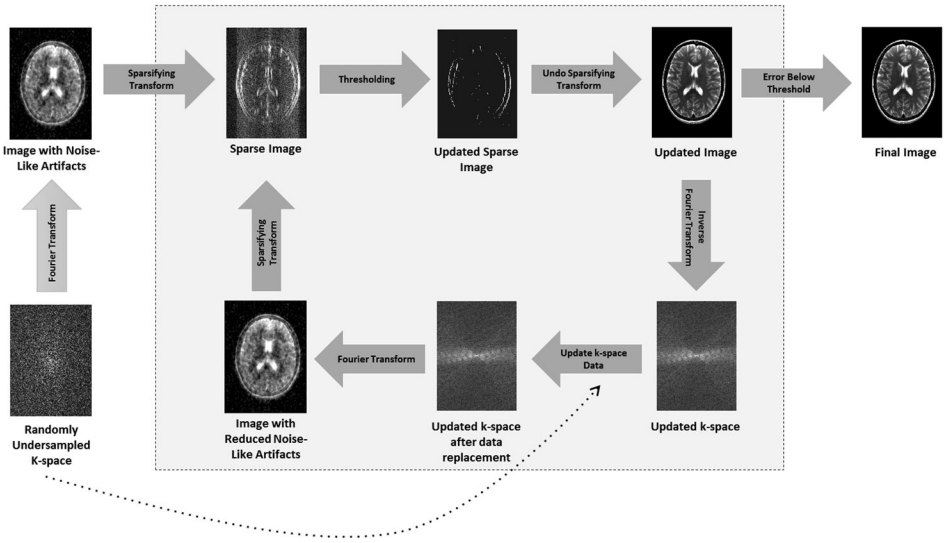

Figure 7.

A schematic of a simplified compressed sensing reconstruction. Randomly undersampled k-space data are collected (bottom left), leading to an image which exhibits noise-like aliasing artifacts (top left). A sparse representation of this undersampled image can be obtained by applying a sparsifying transform such as finite differences, which highlights edges. Because the artifacts look like noise, it is possible to retain most of the significant pixels in the sparse image while removing some noise-like artifacts by thresholding this image. After thresholding, only true edges remain, although some may have been lost in the thresholding process. An updated image is generated by “undoing” the sparsifying transform, and this updated image with reduced aliasing artifacts is converted back to k-space. This k-space may contain data that is different from the collected k-space data after the thresholding step. Therefore, to ensure data consistency, the original k-space data are reinserted into the k-space of the updated image. This updated k-space is then converted into an image, which is now both consistent with the original data and contains reduced aliasing artifacts, and the loop begins again. When the error between the previous iteration of the updated image and the current iteration reaches the stopping criteria set by the user, the iteration loop is broken and the final image is output.

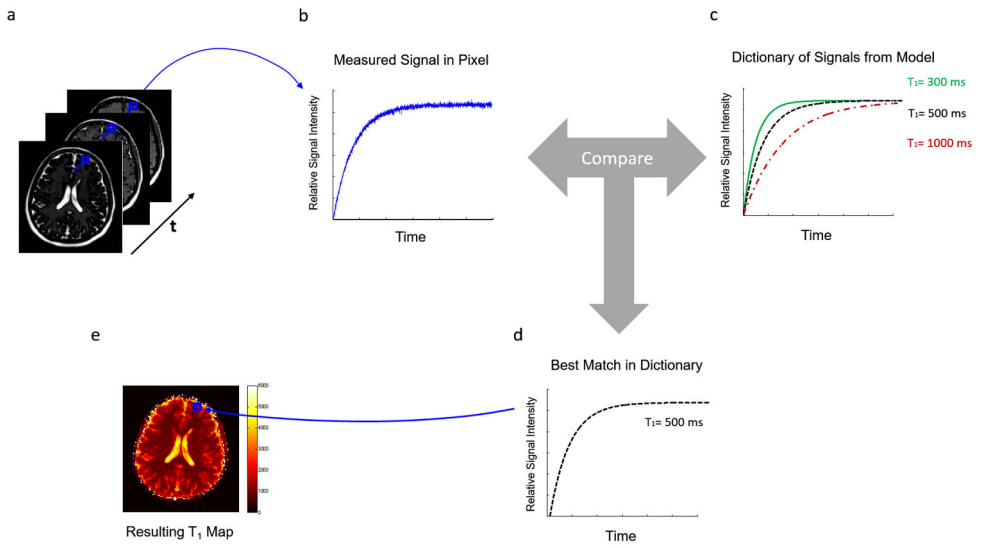

Figure 8.

(a) From a set of rapidly collected undersampled T_1-weighted images, one pixel is selected and examined through time (b). With a knowledge of the underlying physics, a model can be used to calculate all possible signal timecourses for different values of T_1. In this case, the dictionary consists of signals which could arise from T_1 values of 300ms, 500ms, or 1000ms. The actually measured signal is then compared to the signals in the dictionary to find the closest match (d), in this case, the curve for T_1=500ms. (e) The value of 500ms is then assigned as the T_1 value for this pixel. The process is repeated for every pixel of interest to produce a T_1 map.

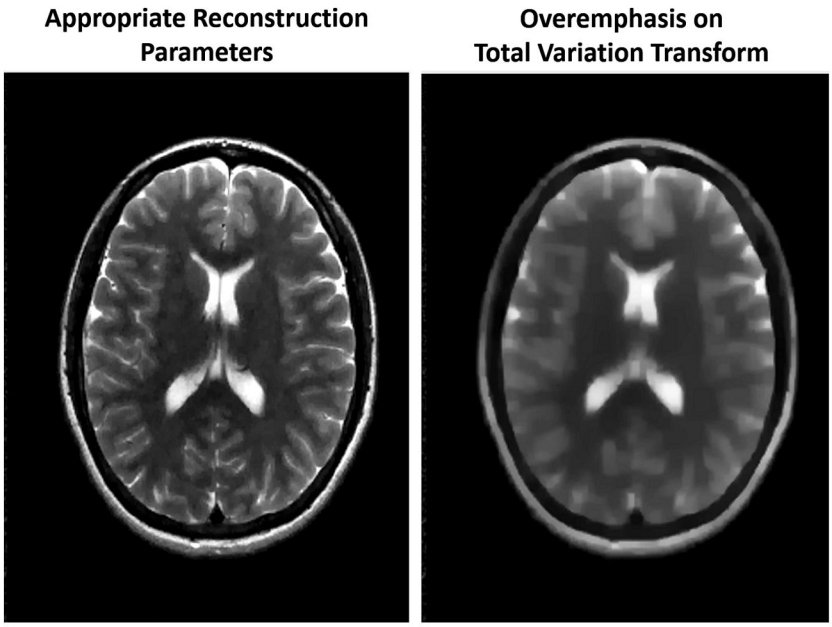

Figure 9.

(left) An image generated using a sparse reconstruction with properly tuned parameters. The image appears clear and with no obvious aliasing artifacts remaining. (right) An image generated with the same data and sparse reconstruction but with a larger regularization term. The overemphasis on the sparsifying transform, in this case total variation, leads to a blurry reconstruction.